

A novel design method for wave-induced fatigue of flood gates

T.N.J. Kleiberg¹, O.C. Tieleman², M. Versluis³, W. Kortlever⁴, E. ten Oever⁵, B. Hofland⁶

Abstract

This paper presents a novel design method to predict fatigue of flood gates due to dynamic wave loading. The accumulation of fatigue damage is predicted probabilistically over the entire lifetime of the structure rather than with a set of normative events. Load events are defined using a joint probability distribution of historical wind and water level data. The random phase-amplitude model is employed to obtain realisations of the wave state for every combination of environmental conditions. Linear wave theory and pressure-impulse theory are used to predict both quasi-steady and highly dynamic wave pressures. The stress response of the structure is predicted with a hybrid semi-analytical and finite element model. By applying a mode matching technique the fluid-structure interaction is solved in a computationally efficient manner. This facilitates the large number of simulations required for a comprehensive fatigue analysis without making concessions in the physical modelling. The fatigue damage is then evaluated with the linear Palmgren-Miner method by applying a rainflow algorithm. A Monte Carlo analysis is performed to estimate the expected fatigue lifetime of the structure. The modular structure of the model routine allows for easy adaptation to other situations where fatigue due to hydrodynamic loading is of interest. The design method is applied to a case study of a flood gate with an overhang inspired by the situation at the Afsluitdijk. Non-fundamental modes are taken into account without simplification of the fluid-structure interaction process and found to be governing for the fatigue damage for the studied case. Moreover, the interference of vibrations due to consecutive wave impacts is shown to have a significant influence on the outcome of the fatigue assessment. For the case study, the design method leads to a 10–20% reduction of the governing fatigue damage compared to a method commonly used in practice. At specific locations on the flood gate fatigue damage is found to be underestimated by current design methods. The presented design method is therefore found to be a significant improvement.

Keywords:


Flood gate, Wave impacts, Fatigue, Hydrodynamics, Fluid-structure interaction

¹joachim.kleiberg@witteveenbos.com, Witteveen+Bos, Deventer, The Netherlands
²o.c.tieleman@tudelft.nl, Delft University of Technology, Delft, The Netherlands
³marco.versluis@witteveenbos.com, Witteveen+Bos, Deventer, The Netherlands
⁴wim.kortlever@rws.nl, Rijkswaterstaat, Utrecht, The Netherlands
⁵erik.ten.oever@bam.com, BAM Infraconsult, Gouda, The Netherlands
⁶b.hofland@tudelft.nl, Delft University of Technology, Delft, The Netherlands

This paper was submitted on 6 January 2022. It was accepted after double-blind review on 10 July 2022 and published online on 10 August 2022.

DOI: <https://doi.org/10.48438/jchs.2022.0017>

Cite as: Kleiberg, T.N.J., Tieleman, O.C., Versluis, M., Kortlever, W., Oever E. ten, Hofland, B. (2022). A novel design method for wave-induced fatigue of flood gates, *Journal of Coastal and Hydraulic Structures*, 2, 17. <https://doi.org/10.48438/jchs.2022.0017>

The Journal of Coastal and Hydraulic Structures is a community-based, free, and open access journal for the dissemination of high-quality knowledge on the engineering science of coastal and hydraulic structures. This paper has been written and reviewed with care. However, the authors and the journal do not accept any liability which might arise from use of its contents. Copyright © 2022 by the authors. This journal paper is published under a CC BY 4.0 license, which allows anyone to redistribute, mix and adapt, as long as credit is given to the authors. 

1 Introduction

Flood gates are commonly used in storm surge barriers and discharge sluices to regulate discharges and prevent flooding. Many of these structures are ageing and increased flood safety standards have made renovation or replacement necessary. As sea levels are expected to rise the hydraulic loads will also become larger and more unpredictable (Groeneweg et al., 2013; Hurk et al., 2006).

Fatigue life estimation plays an essential role in the design process of such gates, which are generally subjected to time-varying loads induced by a variety of sources. Especially wave impacts have the potential to lead to large fatigue damage for a number of reasons. Firstly, they have a relatively high frequency of occurrence. During a single storm event several thousand wave impacts may occur. Secondly, these loads generally involve short but high pressure peaks (Bagnold and Ramkema, 1978; Hofland et al., 2010; Bagnold, 1939), which have the potential to cause significant gate vibrations and lead to a succession of stress cycles after each impact. Fatigue due to wave impacts has for instance proved to be a governing failure mechanism in the design of the more than fifty flood gates at the Afsluitdijk dam in the Netherlands (Rijkswaterstaat, 2020a) (Fig. 1). A situation where this mechanism is of particular interest is that of a flood gate with an overhanging structure. This could for example be the case when a bridge deck is situated just in front of the gate, or when the gate is placed within a culvert. If the water level is sufficiently high, a wave can collide with the bottom of the overhang and cause a pressure spike which results in a highly dynamic response of the gate.

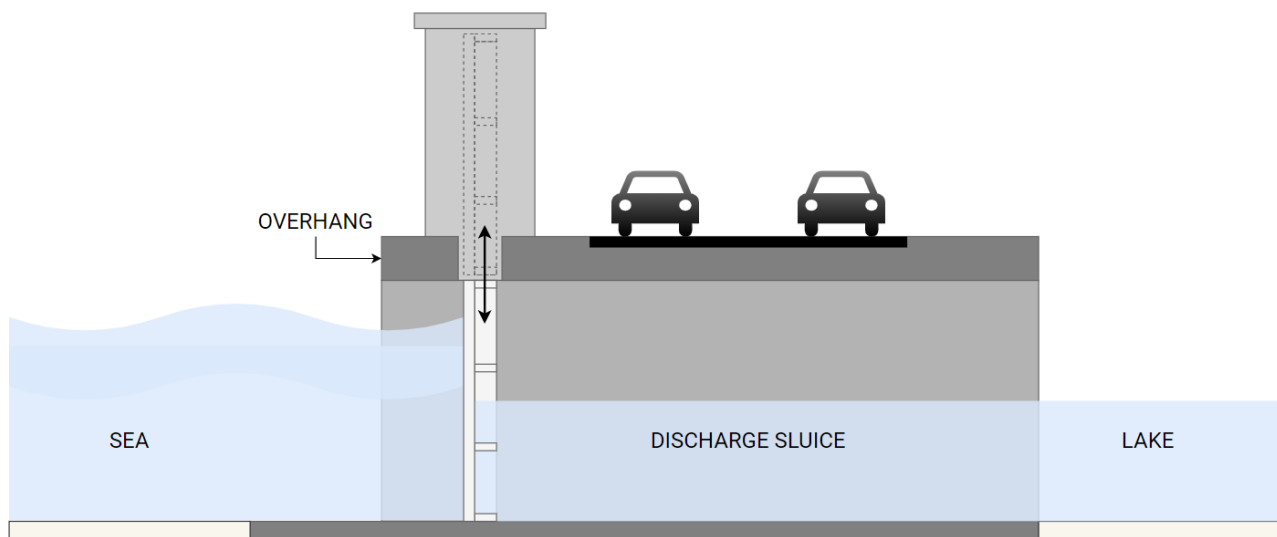


Figure 1: Schematic overview of fluid-structure system with overhang

Fluid-structure interaction makes the prediction of the dynamic behaviour of the gate due to wave impact pressures complex. In addition, this process is accompanied by different sources of uncertainty. Short-term wave statistics are subject to a lot of variance. The variation as well as long-term development of hydraulic boundary conditions introduce further uncertainties. Moreover wave impacts have a highly variable nature (Hofland et al., 2010; Chen et al., 2019; Kortenhuis et al., 1999) in which waves with similar characteristics lead to significantly different peak pressures. Another complicating issue is that the dynamic response cannot always be resolved by looking at individual wave impact loads. As shown by Tieleman et al. (2021), the combined response to consecutive waves should be taken into account. A probabilistic design approach for fatigue which accounts for all of these uncertainties could result in both a safer and more cost-effective design.

The key challenge for such an approach is to accurately model the gate and fluid response in a computationally efficient manner that allows for a large amount of simulations of the entire lifetime of the structure. For reference, the design lifetime of flood gates in the Netherlands is generally around 100 years. Existing methods used in engineering practice tend to rely on finite element simulations which fulfil the requirement of being accurate, but are not sufficiently computationally efficient. For a finite element model the time-domain computation required for a probabilistic evaluation of the dynamic behaviour of a flood gate would be almost an impossible task. Within the field of hydraulic engineering, simulating the dynamic response of a structure for a large number of waves or storms is therefore rarely done in practice. When probabilistic approaches are applied, the wave

loading and structural model are strongly simplified. Within the fields of marine and offshore engineering these type of simulations are more common (e.g. when evaluating the fatigue damage of offshore platforms (Zheng et al., 2020) or the feasibility of dredging or pipe laying operations (Van der Wal and De Boer, 2004)). However, simulating the full dynamic behaviour of a ship or structure for a multitude of storms over the entire lifetime while also analysing the reliability of the system is rare within these fields as well.

Simplified approaches are therefore generally applied in practice. This necessitates limiting either the number of load cases, the accuracy of the response model, or both. Fatigue due to wave loads is often derived from a set of normative storm events. The storm events are subdivided into sets of individual wave impacts according to probability distributions such as the Rayleigh distribution. This means that consecutive wave impacts cannot interfere with each other. Furthermore, the response is only evaluated for a small number of individual wave impacts. The large uncertainties left by these simplifications often lead to conservative assumptions. To model the response of the gate a simplified quasi-static approach is commonly employed in which a dynamic amplification factor (DAF) is applied to account for the effect of the vibrations. This factor is derived from a single degree of freedom representation of the structure (Kolkman and Jongeling, 2007*a*; Cuomo, 2007). Such an approach lacks the precision to capture the three-dimensional vibration behaviour of a gate-fluid system necessary to obtain an accurate prediction of the structural stresses that lead to fatigue damage (Tieleman et al., 2018).

This paper therefore presents a novel design method that evaluates fatigue damage due to confined wave impacts over the lifetime of a flood gate, without making concessions on the number of considered load cases or the accuracy of the response calculation. The methods are based on the previously developed model routine for the evaluation of the ultimate limit state by Tieleman et al. (2021). However, this model routine is adapted to enable the evaluation of fatigue damage by accounting for all expected loads over the lifetime of the structure instead of a single storm event. Furthermore it evaluates complex gate geometries with stiffeners rather than a homogeneous plate. A probabilistic description of the load cases can account for the variable nature of the hydraulic boundary conditions and wave impact loads. Random wave states are derived from the environmental conditions with commonly used spectral shapes from Hasselmann et al. (1973) and Hughes (1984). These realisations are used to derive pressures on the surface of the gate based on a combination of linear wave theory (Airy, 1845) and pressure-impulse theory (Wood and Peregrine, 1997). The response of the dynamically excited gate-system is derived with the semi-analytic method from Tieleman et al. (2018) combined with a FEM-model according to Vorderegger (2019). The stress histories obtained from this combined response model are used to evaluate fatigue by extracting the stress cycles with the Rainflow algorithm (Matsuishi and Endo, 1968) and calculating a fatigue damage factor with the linear damage summation rule from Miner (1945).

This efficient model routine for deriving the fatigue for a given set of environmental conditions is used to probabilistically assess the fatigue lifetime of the structure. First, a simplified joint probability density function is created for the environmental conditions based on historical data and climate change projections. It is then integrated to define a discrete set of load events with an associated probability of occurrence. The fatigue damage contribution and probability of occurrence of each load event is then combined in a Monte Carlo simulation to find an estimate of the projected lifetime of the gate. A case study is performed to demonstrate the benefits of the presented design method. The outcomes are compared to those of commonly applied methods and show a significant improvement in the projection of the fatigue lifetime.

The structure of this paper is as follows. Section 2 describes the model geometry that is considered in this study. Section 3 presents the design routine for a single storm event from deriving the wave state, through the pressure derivation and gate response, to the fatigue calculation. Section 4 then presents the probabilistic lifetime design routine. The case study is elaborated in Section 5. Section 6 discusses the key assumptions and potential improvements of the presented design method. Finally, Section 7 presents the conclusions of this paper.

2 System description

A schematised overview of the system is shown in Figure 2. A discharge sluice is situated between a shallow sea with water level h_S and a lake with water level h_L . The water level at sea is subject to variations due to various sources such as tides and storm surge, while the water level at the lake is considered to be regulated and therefore constant in this study. Variations of the water level on this side could be considered as well within the

presented method however. During a storm event, the water level at sea will be higher than the water level at the lake. A flood gate is therefore installed in the discharge sluice to stop intrusion of sea water when necessary.

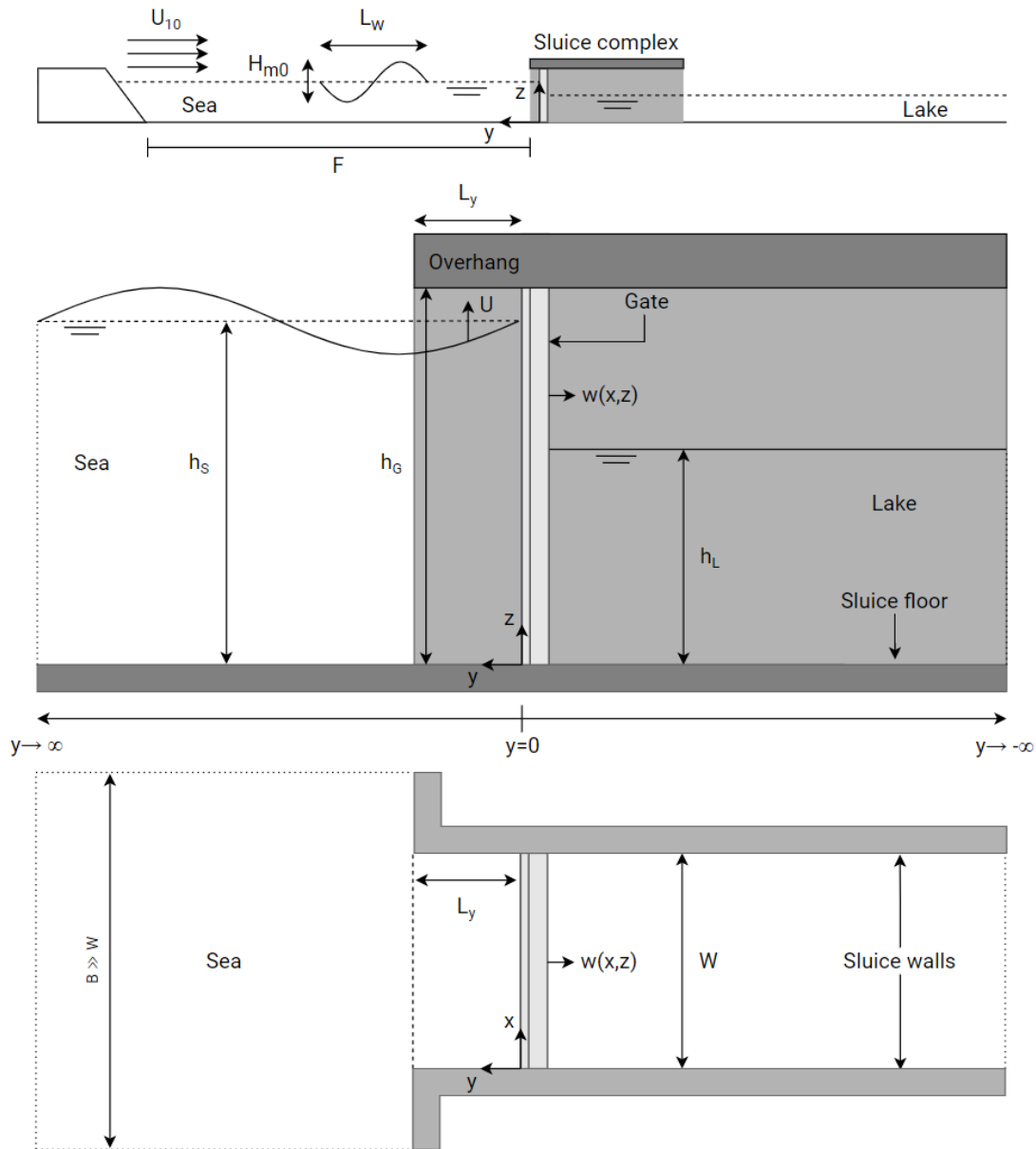


Figure 2: Cross-section of the complete problem (top) and a cross-section (middle) and top view (bottom) of the sluice and gate structure

The width of the gate W [m] is equal to that of the discharge sluice. The gate has a height h_G [m]. At the sea side an overhang is present over the length of the discharge sluice on this side L_y [m]. For the purpose of the hydrodynamic response the sluice extends to infinity, which means the boundaries don't influence the system. The sea is modeled as infinitely wide and long. The walls and floor of the discharge sluice are rigid and impermeable. The water has a free surface everywhere except when constrained by the overhang. The water on both sides is considered to be compressible, irrotational, and inviscid.

The gate consists of a front plate with rectangular stiffeners on the lake-facing side in both the vertical and horizontal directions. The horizontal stiffeners are reinforced with flanges. The geometry of the gate is described parametrically according to the definitions in Figure 3. The gate has a uniform mass density ρ_s [kg/m^3] and modulus of elasticity E [MPa]. Generally, these type of vertical lift flood gates are simply supported at the sides and unsupported at the top and bottom. The gate considered in this paper will also be supported this

way, but the fluid structure interaction (FSI) model from Tieleman et al. (2019a) allows for any combination of geometry and boundary conditions to be evaluated.

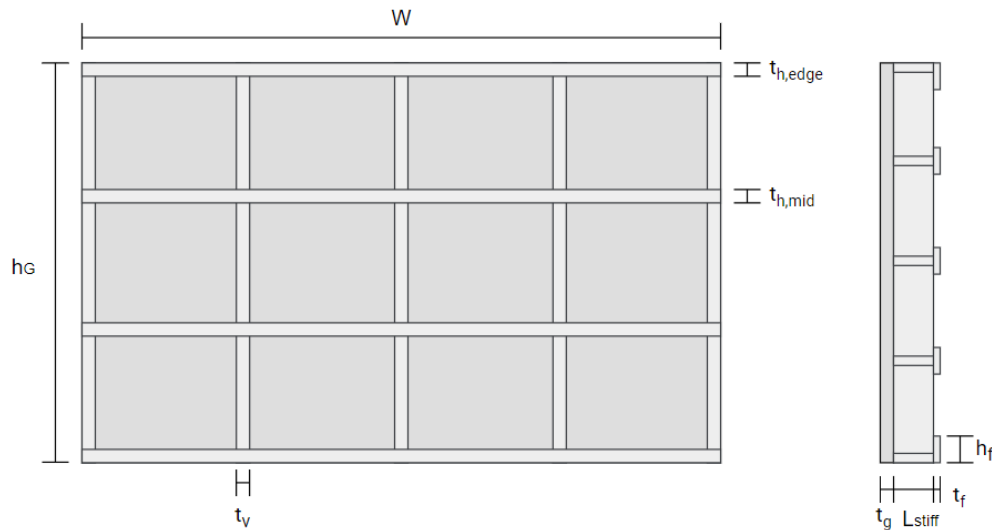


Figure 3: Parametric dimensions of the gate

The gate is subjected to loads by waves at the sea side. These waves are either locally generated by wind over a fetch length F [m] and with a velocity u_{10} [m/s] at 10m height, or swell waves originating further out at sea. The average water depth at sea is assumed constant over the fetch. The waves are confined by the presence of an overhang in front of the gate, which causes pressure spikes and a highly dynamic response. Other loads such as wind, ice or operational loads will not be considered in this study but can be included in the presented design method.

3 Predicting the dynamic response for a single load event

This section describes a model routine to predict fatigue damage for a single load event, corresponding to a wave spectrum that follows from constant environmental conditions (h_S and u_{10}). The probabilistic design method presented in the following section utilises this model routine to predict the expected fatigue lifetime based on the fatigue damage corresponding to each load event and its probability of occurrence.

This model routine combines several existing and recently developed theories. The routine comprises multiple independent modules, as shown in Figure 4. This approach makes it possible to apply different theories within each of these modules when preferred for a specific study, for example higher order wave theory or computational fluid dynamics instead of linear wave theory.

A random wave series is first derived from the environmental conditions. This wave field will be used to create a two-dimensional pressure field on the gate surface for the duration of the load event, from which the response of the gate is then derived by employing a hybrid semi-analytic and finite element fluid-structure interaction model. The resulting stress time series are turned into a fatigue damage factor with the Rainflow algorithm from Matsuishi and Endo (1968) and the Palmgren-Miner method (Miner, 1945).

3.1 Wave field

The wave conditions are predicted in this study based on historic water level and wind data. Historic wave data can also be used directly in combination with water level data. However, for many locations other than the Dutch coast long term and high-resolution wave data is not available. The more general approach based on water level and wind data is therefore presented here.

The theory by Bretschneider (1959) is employed to translate the water level (h_S) and wind velocity (u_{10}) to a JONSWAP variance density wave spectrum (Hasselmann et al., 1973) as a function of the wave frequency

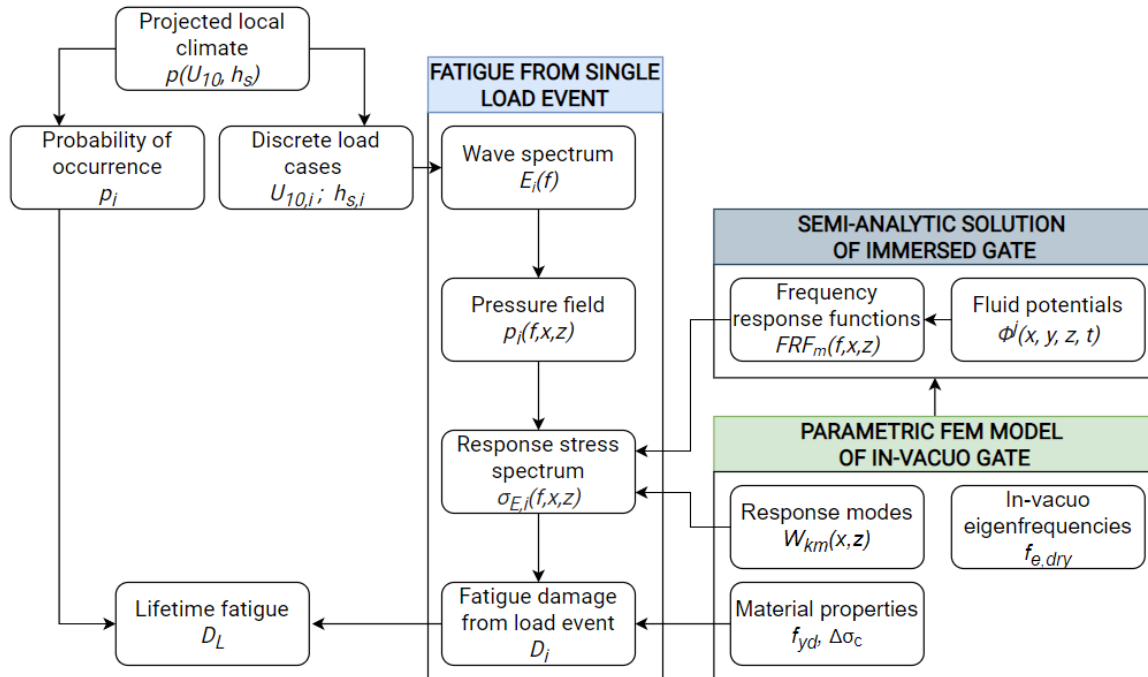


Figure 4: Schematic overview of the design method presented in this paper

f [Hz], given a set of shape parameters and the wind fetch F . More advanced wave models could also be applied within this model routine, for example when considering cases with more complex bathymetries. The waves are assumed to be non-steep and locally generated.

The presented model routine is able to evaluate pressure fields which are not uniform over the width of the gate. However, in this paper all waves are considered to be long-crested and have a perpendicular angle of approach to the discharge sluice and gate. The wave pressures will therefore be uniform across the width. The wave state is also assumed to be fully developed in all cases.

To account for the shallowness of the sea, the JONSWAP spectrum is modified with a depth correction factor such as the one given by the TMA spectrum from (Hughes, 1984). This adds a dependence on the local water depth and truncates the JONSWAP spectrum to account for the effect of bottom friction on the wave state. Figure 5 shows examples of both spectra.

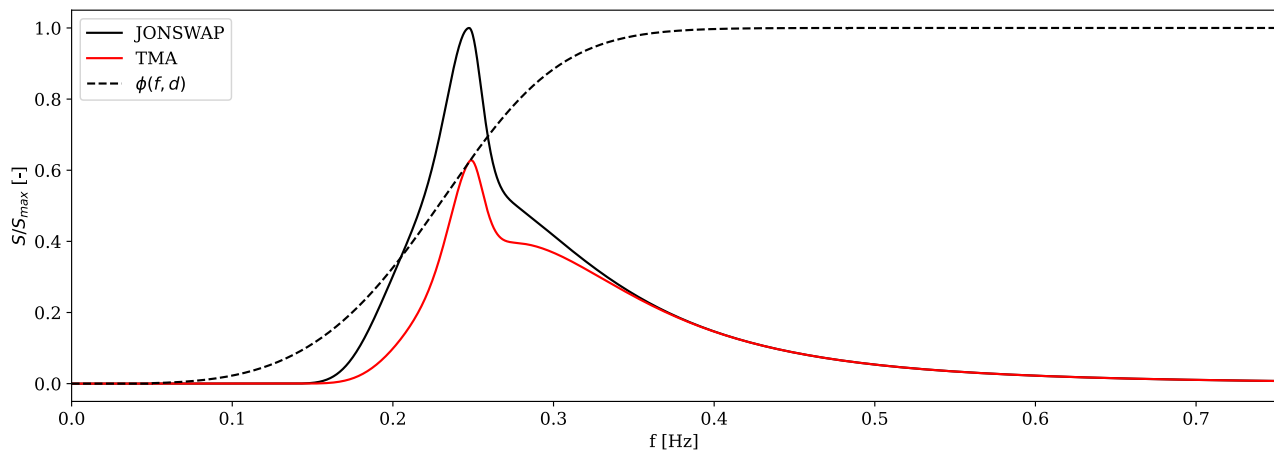


Figure 5: Examples of JONSWAP and TMA amplitude spectra for $h_S = 7.5\text{m}$ and $u_{10} = 10\text{m/s}$

The result is a variance density spectrum $E(f)$ [m^2/Hz], which defines the amount of spectral energy concentrated at every frequency. A time domain wave series may be derived from the spectrum by means of the

random phase-amplitude model (Holthuijsen, 2007). For this purpose, realisations $E_i(f)$ of the spectrum are generated by adding a random phase to each frequency. For non-steep linear waves, this phase is uniformly distributed (Holthuijsen, 2007), denoted by $U(0; 2\pi)$.

Because the gate also reflects the waves back, the water level at the surface of the gate can be up to twice as high. The strength of the reflection is determined by the reflection coefficient c_r [-], which can range from 0 to 1 depending on the geometry of the structure. De Almeida and Hofland (2020b) showed that for vertical gates with an overhang a reflection coefficient of 1 is a reasonable assumption because the incident wave is not influenced by the overhang during the half-period before the wave impact occurs. Therefore $c_r = 1$ will be assumed in this paper as well.

$$E_i(f) = (1 + c_r) \cdot E(f) \cdot e^{-i \cdot U(0, 2\pi)} \quad (1)$$

The peak frequency of the resulting spectrum is found by determining the frequency with the highest energy content. The significant wave height follows from $H_{m0} = 4\sqrt{m_0}$, where the spectral moment m_0 [m^2] follows from Equation 2 for $m = 0$.

$$m_n = \int_0^\infty f^n E_i(f) df \quad (2)$$

3.2 Hydrostatic and wave pressures

The wave spectrum will now be used to derive a pressure field over the surface of the gate. The pressure is subdivided into three distinct types, visualized in Figure 6. The mean water levels at either side of the gate impose a constant hydrostatic pressure on the gate which increases with depth according to Equation 3:

$$p_{hs}(x, y = 0, z, t) = \rho g z \quad (3)$$

This is represented in the frequency domain as a load with frequency zero. The fluctuations due to quasi-steady wave pressures will be added to this static average by applying linear wave theory (Airy, 1845) (only valid for non-steep waves) to the previously derived wave spectrum at every coordinate on the gate surface.

$$p_{qs}(x, y = 0, z, t) = \rho g a \frac{\cosh k(z + h)}{\cosh kh} \cos \theta \quad (4)$$

The pressure due to impulsive wave impacts is very unpredictable, but with the pressure-impulse theory

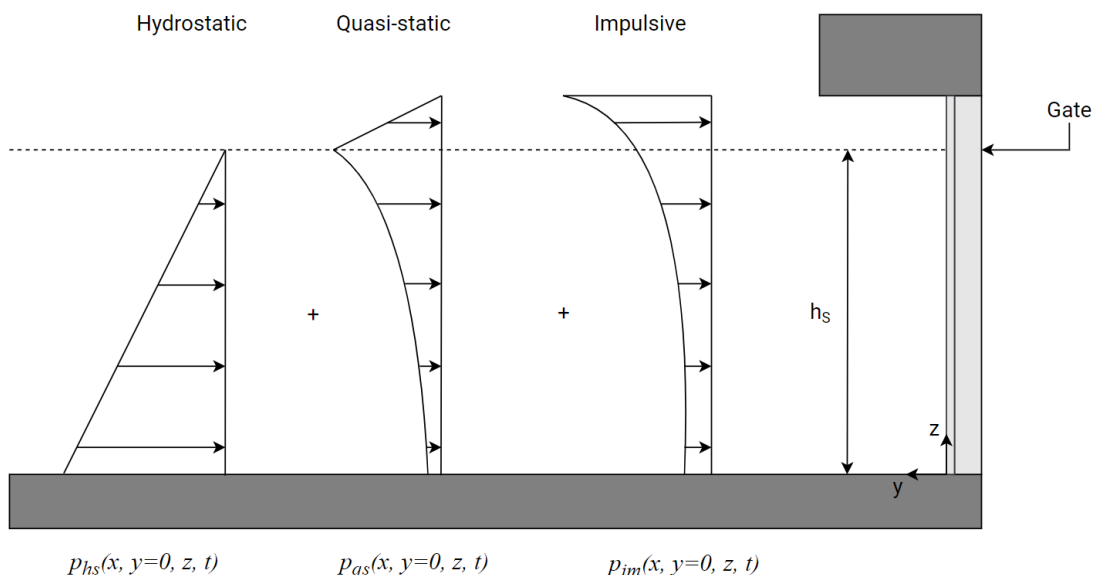


Figure 6: Components of total hydraulic pressure.

from Wood and Peregrine (1997) it can be probabilistically described. In Equation 5 the geometry-dependent dimensionless pressure-impulse shape $\bar{P}(x, y = 0, z)$ [-] is combined with a pressure peak shape, the impact

velocity of the water surface U_w [m/s], and a correction factor for the compressibility of entrapped air $1 < \beta_{im} < 2$ [-] (De Almeida and Hofland, 2020b). The result is a pressure distribution over the surface of the gate.

$$\bar{P}(x, y = 0, z) = \frac{P_{im}(x, y = 0, z)}{\beta_{im}\rho_w U_w L_y} = \frac{\int_{t_0}^{t_1} p_{im}(x, z, t) dt}{\beta_{im}\rho_w U_w L_y} \quad (5)$$

Four examples of the dimensionless pressure-impulse shape over the height of the gate are plotted in Figure 7 for different values of L_y . The integral from Equation 5 can be solved by assuming a shape for the pressure impact, which Chen et al. (2019) shows can be represented with reasonable accuracy as a symmetric triangle. The base of this triangle is a probabilistic impact duration $\tau = t_1 - t_0$ [s], which means the peak pressure can be described by:

$$\int_{t_0}^{t_1} p_{im}(x, z, t) dt = \frac{1}{2} \tau p_{peak} \quad (6)$$

The experiments of De Almeida and Hofland (2020b) have validated the model for relatively short overhangs relative to the wave length L_w ($12.1 < L_w/L_y < 43.6$), low steepness, and non-breaking conditions.

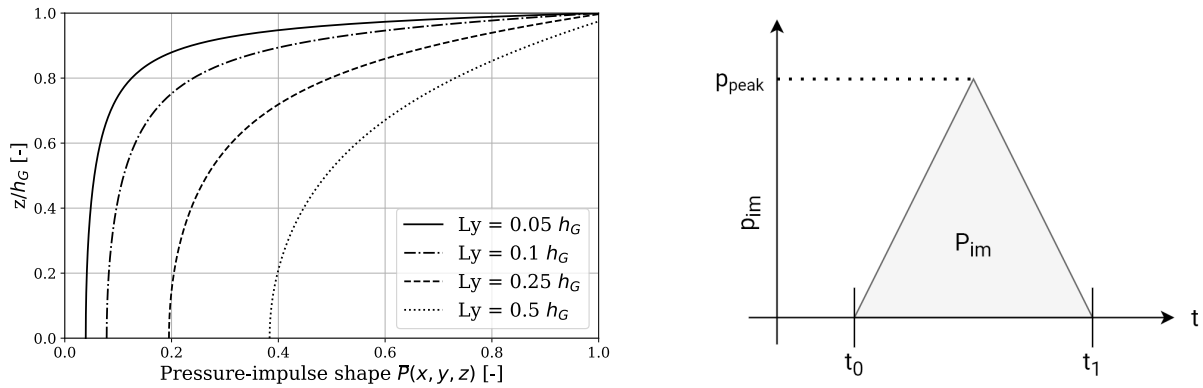


Figure 7: Dimensionless pressure impulse shape for different values of L_y (left) and the triangular impact pressure shapes over time (right)

The upward impact velocities of the water U_w surface are found by taking the derivative of the wave field every time it crosses the elevation of the overhang in the upwards direction. For β_{im} , findings in De Almeida and Hofland (2020b) suggest a normally distributed value with a mean of 1.17 and a standard deviation of 0.11 for standing waves. De Almeida and Hofland (2021) expand this to irregular waves by first introducing a Γ -factor from which the correction factor β can then be calculated:

$$\Gamma = U_{w,1\%}^2 L_m / g L_y^2 \quad (7)$$

$$\beta = 2 - e^{-0.16\Gamma} \quad (8)$$

L_m [m] is the mean wave length associated with the mean wave period T_{m02} [s], which is defined in Equation 9 based on the spectral parameters from Equation 2 (Holthuijsen, 2007).

$$T_{m02} = \sqrt{\frac{m_0}{m_2}} \approx 1,1 T_p \quad (9)$$

For the 1%-wave of an irregular wave field, the corresponding impact velocity $U_{w,1\%}$ [m/s] follows from Eq. 10 (whose derivation in De Almeida and Hofland (2020a) presupposes that the waves are sufficiently high to reach the overhang).

$$U_{w,i} = \frac{2\pi}{T} \sqrt{\left((1 + c_r) \frac{H_i}{2} \right)^2 - (h_s - h_G)^2} \quad (10)$$

Based on the results shown in Figure 16 of De Almeida and Hofland (2020a), the value for β will be randomly drawn from a normal distribution where the mean is given by Equation 8 and whose standard deviation is estimated from the 90% confidence intervals as 0.12. Because this definition of β is based on the highest 1% of wave impacts, it can be used as a conservative estimate for the compressibility correction factors of every wave in the spectrum.

A distribution for the probabilistic impact duration τ of each impact will be based on the findings from the scale experiments by De Almeida and Hofland (2021). For a short overhang ($h_S/L_y = 6$), values for τ were found to be approximately triangularly distributed with a lower limit of 5 ms, a mode of 75 ms, and an upper limit of 200 ms. These values are Froude-scaled to the scale under consideration by a scaling factor of $\gamma^{0.5}$, with $\gamma = L_y/0.1$ as the overhang in the scale experiments by De Almeida and Hofland (2021) had a length of 0.1 m. It should be noted however that Froude's law is not necessarily accurate here, as near the atmospheric pressure non-linear interactions between the air and water pressures start to play a role. Depending on the way air is entrapped below the overhang, the impact durations can be both shorter or longer than predicted (Bagnold and Ramkema, 1978). Research on the dependence between air entrapment and different wave properties is ongoing based on the results from De Almeida and Hofland (2021). Here, it is assumed the variation for irregular wave conditions can be fully captured in the triangular distribution of the impact duration. Depending on the outcome of further research, it may be necessary to define distributions dependent on the wave conditions.

Evaluating Equation 5 for these random variables gives a set of pressure peaks. Adding the all together at their respective moments of impact then results in a single pressure field $p(x, z, t)$ [Pa] over the surface of the gate. Finally, the quasi-static and impulsive pressure fields are combined to give a description of the combined pressure field over the duration of the load event. A random realisation is plotted in Figure 8, which shows the impulsive pressure peaks alongside the slower fluctuations from the quasi-static wave pressures.

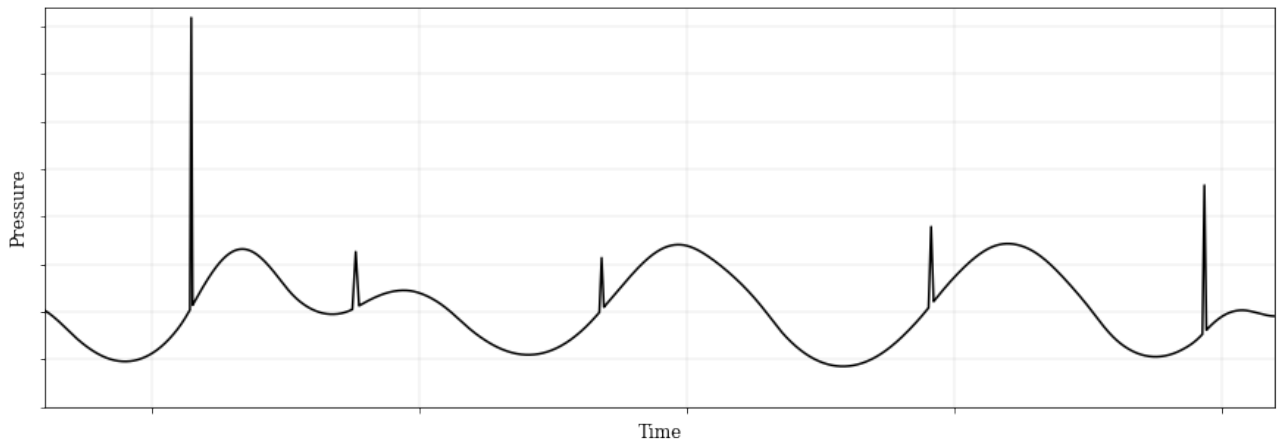


Figure 8: Combined depth-integrated pressure time series of all three pressure components: the hydrostatic, and quasi-steady and impulsive wave pressure

3.3 Dynamic response of the immersed gate

A recently developed hybrid semi-analytical and finite element method by Tieleman et al. (2022) is employed to predict the response of the gate immersed in fluid. The method of solution is based on a substructuring mode matching technique similar to Tsouvalas and Metrikine (2014, 2016) and Leblond et al. (2009). Tieleman et al. (2022) derives a semi-analytical solution for the fluid-structure interaction problem. The motion of the in-vacuo gate structure and the corresponding stresses are described in terms of modal coefficients:

$$\tilde{u}(x, y, z, \omega) = \sum_{k=1}^{\infty} A_k(\omega) U_k(x, y, z) \quad (11)$$

$$\tilde{\sigma}_{ij}(x, y, z, \omega) = \sum_{k=1}^{\infty} A_k(\omega) S_{k,ij}(x, y, z) \quad (12)$$

in which u [m] denotes the displacement of the gate structure at a certain discretized point, the coefficients A_k [m] denote the amplitudes of the corresponding gate displacement modes U_k [-] and stress modes $S_{k,ij}$ [-], with $ij = x, y, z, xy, xz, yz$ denoting each of the directional stresses. The motion of the fluid in the domains at either side of the gate is described in a similar matter. The semi-analytical solution then solves the modal coefficients of both the structure and fluid for the joint system in the frequency domain. Any time-domain force can then be applied to the model with the use of a Fourier transform. The main computational advantage of the mode matching technique lies in the ability to store and reuse partial results in contrast to the step-wise calculation in finite element (FE) methods. Even when evaluating a large number of loads, the frequency response function of the gate fluid system only has to be computed once.

The model uses the in vacuo gate modes, fluid modes, and the corresponding frequencies as input. The fluid modes are found by solving the partial differential equation of the fluid motion analytically. A structural finite element model is employed to find the modal shapes and frequencies of in-vacuo gate displacement and corresponding stresses. Any finite element software package which uses the theory of elasticity can be used for this purpose. For this study, SCIA Engineer 2021 is employed. This procedure is straightforward and requires minor computational effort since the interaction with the fluid is not evaluated in the finite element model, but with the semi-analytical approach.

Damping due to fluid compressibility and surface waves is an implicit part of the fluid-structure interaction model. However, for the frequencies and water depths involved with wave impacts on flood gates these damping effects are usually insignificant (Tieleman, 2016; Tieleman et al., 2019a). Furthermore, a material damping factor η [-] can be included directly in the semi-analytical solution. In this study, the application of damping is limited to this material damping factor. However, other types of damping, for instance at the supports of the flood gates, could be modelled within the finite element model of the in-vacuo gate. This would result in complex modal shapes and frequencies as input to the semi-analytical solution.

The wave impact forces or any other time-varying loads are modelled as an external pressure on the surface of the gate. One of the key assumptions of this model approach is therefore that the impact force does not affect the still water level. In Tieleman et al. (2019b) this was discussed to be a reasonable assumption for the time scales involved in impulsive wave impacts. Time series of the wave impact load are Fourier transformed to the frequency domain to determine the frequency response of the system. An inverse Fourier transform is then applied to obtain a time series of the gate response in terms of deflections and stresses.

3.4 Fatigue of the structure

The final step within the model routine is to predict the fatigue damage. Various methods exist to evaluate the fatigue lifetime of a structure in the time domain, such as peak counting, level-crossing counting, range-mean counting and rainflow counting (RFC) (Benasciutti and Tovo, 2006; Rychlik, 1993). A frequency domain stochastic fatigue analysis is an alternative approach that is often chosen by engineers to avoid numerically costly time-domain simulations. When the stochastic stress process is narrow-banded and Gaussian, its amplitudes follow the Rayleigh distribution. Therefore, the accumulated fatigue can be calculated by integrating the probabilistic function (Zheng et al., 2020; Newland, 2012). For wide-banded processes, an analytic solution does not exist and application of the spectral method is less straightforward.

When sufficiently long stress series are available, the time-domain RFC analysis (Downing and Socie, 1982) for fatigue evaluation is generally the first choice (Zheng et al., 2020). The numerical efficiency of the developed model allows for such an evaluation. The RFC is therefore applied as the cycle counting method in this study. For this purpose, the predicted directional stresses $\tilde{\sigma}_{ij}(x, y, z, \omega)$ [Pa] in the frequency domain are inverse Fourier transformed to obtain the time domain response. These directional stresses are then translated to the type of stress relevant for the fatigue criterium. In this study, fatigue is evaluated by means of the maximum principal stress in accordance with the Eurocode (CEN, 2012) in order to preserve direction. The signed Von Mises stress is applied as an alternative in practice as well.

The accumulated fatigue damage is then predicted with the well-known tri-linear logarithmic S–N curve of the material and the Palmgren–Miner rule (Miner, 1945), which compares the stress cycles extracted from the time series with the capacity defined by the S–N curve (See Eq. 13). The resistance of a material or connection is typically characterised by its detail category $\Delta\sigma_c$ [MPa] as defined in the Eurocode (CEN, 2012), which represents the resistance at $N_c = 2 \cdot 10^6$ [-] and allows the rest of the curve to be calculated.

$$D = \sum_{i=1}^k \frac{n_i}{N_{c,i}} \quad (13)$$

where D [-] is the fatigue damage factor, $N_{c,i}$ [-] the allowable amount of a given stress cycle i , and n_i [-] the amount of these stress cycles found in the time series. D indicates how much of the fatigue capacity of the material was depleted by the load event. When D exceeds 1, the element under consideration has failed.

4 Probabilistic lifetime analysis

The high computational efficiency of the model routine presented in the previous section, makes it possible to consider a large number of load events to characterise the stresses in the gate over the lifetime of the structure. This section proposes a probabilistic method to perform a lifetime fatigue damage assessment of a flood gate subjected to wave impacts utilising this efficiency.

Section 4.1 describes how the relevant load cases are derived within this method. A way to further optimise the computational efficiency of the method by filtering irrelevant load cases and choosing a suitable resolution is presented in 4.2. Finally, paragraph 4.3 shows how the fatigue lifetime follows from the presented method.

4.1 Load event derivation

The fluctuations of the water surface relevant for this study can be subdivided into three types:

- Periodic short-term changes, e.g. local wind waves or swell;
- Periodic long-term changes, e.g. tides or storm surge;
- Cumulative long-term changes like sea level rise or land subsidence which change the mean water depth over time.

These fluctuations will be accounted for in different ways within the presented probabilistic method. Historical wind- and water level data of at least hourly intervals are used to generate load cases with representative values for the time-averaged water level h_S and average wind velocity U_{10} . This data is publicly available for many locations along the Dutch coast. The short term water level fluctuations will be determined with the use of a wave spectrum based on these two parameters, as described in paragraph 3.1. Because the periods of tides, storm set-up, atmospheric pressure changes, and other long-term effects are generally much longer than an hour, the hourly averages of the mean water level and wind velocity may be employed to predict short-term water level fluctuations.

The long-term periodic changes are expected not to cause fatigue damage due to their quasi-static nature and low cycle count, and are therefore not included in the fatigue assessment. The validity of this assumption can be verified for any specific case. If necessary, the stress cycles caused by these fluctuations can be added to the fatigue damage assessment. Effects that accumulate over time, like climate change or soil settlement, are included separately within this method. These effects are described stochastically by separate probability distributions which define the likelihood that a given relative water level increase occurs at a random point during the lifetime of the gate, and will be combined with the de-trended historical data.

First, probability density functions are fitted to the historical data. When tides are present, sea water levels generally resemble a bi-modal Gaussian distribution. The wind velocities tend to follow a skewed extreme value distribution. The water level distribution is adjusted for long-term effects such as climate change and soil subsidence. If a linear increase over time is assumed the probability distribution of these effects will be uniform. The uniform distribution will range from 0 (at the start of the lifetime) to h_{SLR} [m], which is the expected sea level rise at the end of the lifetime. For coastal structures in the Netherlands, h_{SLR} is generally assigned a fixed value based on a certain climate scenario. More complex distributions that take into account multiple sea level rise scenarios and corresponding probabilities could also be applied within the presented approach however. The design water level probability distribution $f_H(h_S)$ is obtained by performing a convolution of the original

fitted distribution f_1 and the climate change distribution f_2 .

$$f_H(h_S) = \int_{-\infty}^{\infty} f_1(\iota) f_2(h_S - \iota) d\iota \quad (14)$$

The climate scenarios for the Netherlands do not predict a change in wind climate within this century (Hurk et al., 2006). The historical wind data is therefore not adjusted for climate change in this study. However, a similar procedure as for the water levels could be applied to incorporate different scenarios and related probabilities.

Next, the water level and wind distributions are combined into a joint probability density function $f_J(h_S, U_{10})$. The amount of correlation is characterised with the correlation coefficient from Pearson (1895). Depending on the nature of the data independence can be assumed, or a correlation can be applied to either the entire distribution or just the upper tail events.

Next, this continuous joint probability density function will be discretised into a set of two-dimensional segments, each of which will be characterised by a representative load case. After discretisation, the data will look something like Figure 9. The representative values $h_{S,j,k}$ and $U_{10,j,k}$ for any segment (j, k) are obtained by calculating the expected value of $f_J(h_S, U_{10})$ over the intervals $(H_j < h_S < H_{j+1}), (U_k < U_{10} < U_{k+1})$:

$$h_{S,j,k} = \frac{\int_{H_j}^{H_{j+1}} \int_{U_k}^{U_{k+1}} h_S \cdot f_J(h_S, U_{10}) dU_{10} dh_S}{\int_{H_j}^{H_{j+1}} \int_{U_k}^{U_{k+1}} f_J(h_S, U_{10}) dU_{10} dh_S} \quad (15)$$

$$U_{10,j,k} = \frac{\int_{H_j}^{H_{j+1}} \int_{U_k}^{U_{k+1}} U_{10} \cdot f_J(h_S, U_{10}) dU_{10} dh_S}{\int_{H_j}^{H_{j+1}} \int_{U_k}^{U_{k+1}} f_J(h_S, U_{10}) dU_{10} dh_S} \quad (16)$$

The probability associated with that segment is found by integrating the joint probability density function over that interval.

$$p(H_j < h_S < H_{j+1}, U_k < U_{10} < U_{k+1}) = \int_{H_j}^{H_{j+1}} \int_{U_k}^{U_{k+1}} f_J(h_S, U_{10}) dU_{10} dh_S \quad (17)$$

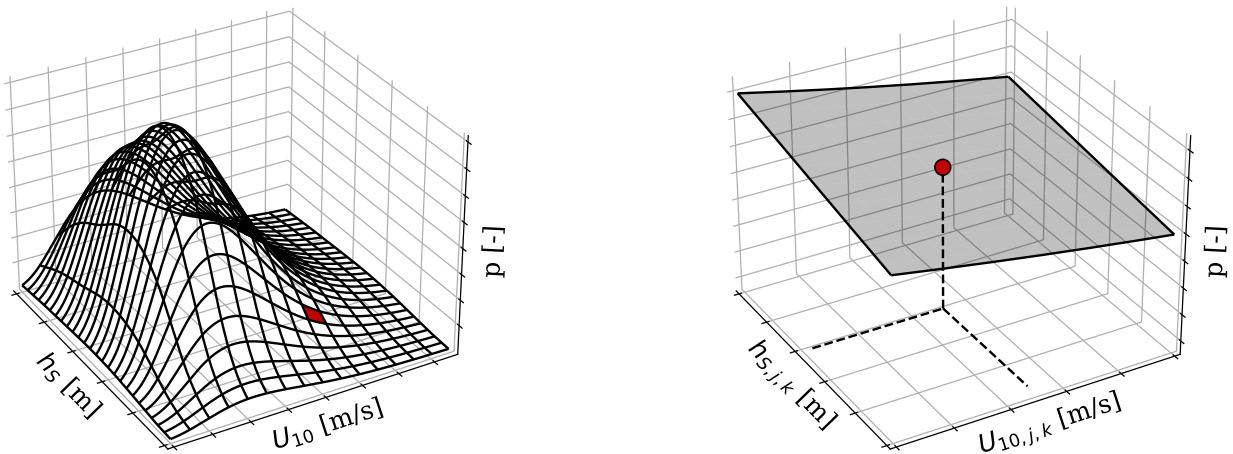


Figure 9: Left: Example joint probability density function of historical data for h_S and U_{10} . Grid lines indicate discrete load cases. Right: Single discrete load case and its representative values.

This results in a set of load cases characterised by representative values for h_S and U_{10} as well as a probability of occurrence. The response of the gate to each of these load cases is then predicted based on the model routine presented in Section 3.

4.2 Load case resolution and filtering

This paragraph provides a method to determine the optimal load case resolution based on convergence of the solution. Methods to filter the list of load cases will also be discussed, to increase the efficiency of the lifetime fatigue analysis.

The choice for the size of the segments is a trade-off between required computational effort and accuracy. A smaller segment size results in a larger number of simulated load cases. The resolutions of the two variables are defined as:

$$\Delta_{h_S} = H_{j+1} - H_j \quad (18)$$

$$\Delta_{U_{10}} = U_{k+1} - U_k \quad (19)$$

The accuracy is assessed with a resolution refinement procedure comparing the standard deviations of a large amount of repetitions randomly picked from within the segments. The resulting error has two sources; variance caused by the probabilistic nature of the wave field and wave impact models applied, and variance caused by the range of possible inputs. For narrower resolutions the randomly picked values will show less divergence. The lower limit for the resolution is zero, in which case only the variance inherent in the model plays a role. This therefore serves as a baseline which can only be asymptotically approached. In order to test convergence, the fatigue analysis is first run N times for the representative values of h_S and U_{10} , which will result in a normally distributed set of fatigue damage values. Then, the fatigue analysis is run N times for random values in a range of Δ_{h_S} [m] by $\Delta_{U_{10}}$ [m/s] around the representative values (i.e. the part of the distribution those values are representing). The standard deviations of these two sets of results are then compared to see how closely the results of the representative values match those of the randomly picked values. This procedure is repeated with increasingly small resolutions until the standard deviations converge. An example of this procedure is given in Section 5.

The load cases are filtered to further improve the computational speed of the presented method. Certain load cases are highly unlikely to occur and can therefore be discarded, while others cause such small loads such that they do not contribute significantly to the lifetime fatigue damage (i.e. all of the stress cycles are below the cut-off limit of the S-N curve).

The very infrequent cases can be filtered out based on their expected probability of occurrence. A common maximum normative return period for loads on hydraulic structures in the Netherlands is 10.000 years. Cases with a longer expected return period are filtered out. If the lifetime analysis (Section 4.3) shows that rare events do contribute significantly this horizon could be extended. This provides the following filtering criterion based on the expected hourly rate of occurrence:

$$p_{\min} < (10.000 \cdot 365.25 \cdot 24)^{-1} = 1.14e^{-8} \quad (20)$$

In order to filter cases based on their contribution to fatigue damage, a statistical property of the wave spectrum will be used to avoid running calculations for all of these cases. Load events where the sum of the statistical maximum wave height and the highest water level does not exceed the elevation of the overhang (h_g) will be removed from the data-set.

The statistical maximum wave height produced by a random realisation of a wave spectrum i is $H_{max,i} \approx 2H_{m0,i}$ [m] (Holthuijsen, 2007). Accounting for reflection, this gives a maximum expected water elevation of $\frac{1}{2}H_{max,i}(1+c_r)$. This results in the following limit for filtering cases that have a low probability of wave impacts occurring:

$$h_s + \frac{1}{2}H_{max,i}(1+c_r) < h_G \quad (21)$$

For these load cases, it is very unlikely that wave impacts on the overhang occur. It is expected that load cases without wave impacts have no or a minor contribution to the fatigue lifetime damage. This assumption is verified for the case study performed in Section 5. All load cases which were filtered based on this criterion did not contribute to the fatigue damage.

4.3 Fatigue damage accumulation over lifetime

The model routine described in Section 3 is now employed to predict the response of the gate for each load case with associated representative values $U_{10,i}$ and $h_{S,i}$. This results in a fatigue damage factor D_i for every

load case i . The associated probability of occurrence $p(D_i)$ [-] follows from the fitted joint probability density function as discussed in paragraph 4.1. The expected lifetime fatigue damage factor D_E [-] then follows from:

$$D_E = T_L \cdot \sum_{i=1}^N p(D_i) \cdot D_i \quad (22)$$

in which N is the number of distinct discrete load cases following from the discretization of the joint probability density function. T_L [-] is the total number of load events that occurs during the simulation period, which would generally be the lifetime of the structure. Depending on the chosen load case duration and lifetime this is typically in the order of $10^5 - 10^8$ events. The fatigue lifetime of the structure is the duration for which the accumulation of load events leads to fatigue failure ($D = 1$). This lifetime can be found by gradually increasing the simulation period and the corresponding load events.

Above estimate ignores sampling uncertainty: by random chance rarer events can occur more or less frequently than on average in certain lifetime simulations. For a probabilistic assessment that includes this effect, a Monte Carlo analysis is therefore performed. Here, load cases are sampled independently based on their probability of occurrence. The fatigue D associated with the randomly picked load cases is cumulatively added until failure occurs (at $D = 1$). The Monte Carlo simulation repeats this process a certain number of times. Based on the resulting lifetime distribution, a design value for the fatigue lifetime of the structure can be found by determining the lower 95th percentile (or any other desired confidence level). See paragraph 5.3 for an example.

The outcome of this simulation is presented in terms of a probability curve of the fatigue lifetime of the flood. However, the same analysis also provides a prediction of the failure probability due to fatigue in each year over the lifetime of the structure. This failure probability will naturally increase of the lifetime. Such a prediction may be needed for safety assessments of flood gates.

5 Case study

The presented method is now applied to a case to demonstrate its purpose and to analyse the results and their implications. This case is hypothetical but based to some extent on the Afsluitdijk renovation project. The Afsluitdijk is a closure dam in the Netherlands that separates the IJsselmeer lake and the Wadden Sea. The water level of the lake is controlled by the two discharge sluices at Den Oever and Kornwederzand. The discharge sluice at Den Oever is located at the south-western side of the Afsluitdijk is being renovated and expanded at the time of writing. The gates considered in this case study have a geometry comparable to the existing gate, but with somewhat more straightforward supporting beam elements. The gates are required to have a design lifetime of 80 years from 2020 to 2100.

Table 1 shows the geometry parameters as defined in Figures 2 and 3 along with the material properties of the gate. The gate is simply supported at its sides ($x = 0; x = W$) and unsupported at the top and bottom ($z = 0; z = h_G$). The gate has six vertical stiffeners and seven horizontal ones. The in-vacuo modes of this gate were calculated with an eigenvalue analysis of a parametric SCIA Engineer model. Figure 10 shows the normalised maximum principal stress distributions for four modes of interest.

Table 1: Geometry parameters (deterministic) of the case study

Symbol	Description	Value	Unit	Symbol	Description	Value	Unit
Geometry				Material			
W	Gate width	10	m	ρ_s	Density of steel	7,850	kg/m ³
h_G	Gate height	7.5	m	E_s	Young's Modulus steel	210	GPa
t_G	Skin plate thickness	0.02	m	f_{yd}	Yield strength	355	MPa
t_v	Vert. stiffener thickness	0.02	m	σ_C	Detail category	100	MPa
t_h	Hor. stiffener thickness	0.02	m	ζ	Damping ratio	0.02	-
L_v	Stiffener length	0.65	m	M_G	Gate mass	22,500	kg
h_f	Flange height	0.2	m				
t_f	Flange thickness	0.02	m				
L_y	Overhang length	1	m				

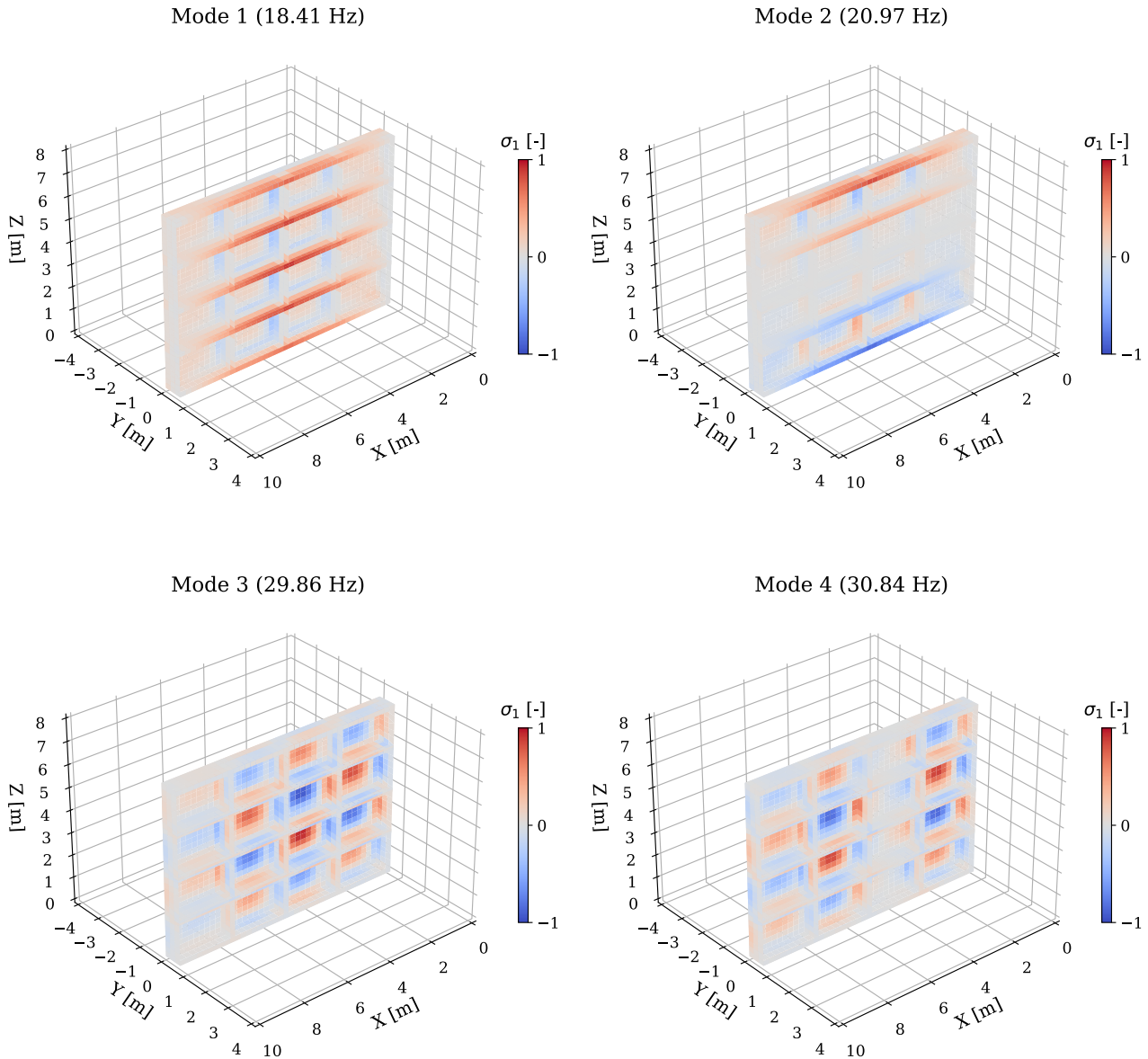


Figure 10: Normalised maximum principal stress distributions for four selected in-vacuo modes of the gate

5.1 Load event derivation

The Wadden Sea experiences tides in addition to atmospheric water level fluctuations. The Wadden Sea has a complex bathymetry with both shoals barely below the mean sea level and gulleys with a depth of about 25 m. However, for the purpose of predicting the generation of local wind waves it is schematised to have a constant average initial depth of 5 m over a fetch of 30 km (roughly the perpendicular distance to the barrier islands). The water level at the lake is constant with a water depth in the sluice of 4 m. It is assumed that the barrier islands and shoals block swell waves generated in the North Sea from reaching the discharge sluices. Only the waves from the sea side are regarded in this case study.

Water level and wind data is obtained from measurement stations operated by Rijkswaterstaat and the Royal Netherlands Meteorological Institute (KNMI). Historical water levels h_S have been measured at the location of sluice complex Den Oever (Rijkswaterstaat, 2020b). Wind data U_{10} is obtained from the measurement station De Kooy, which is located 16.5 km to the west (KNMI, 2020) of the discharge sluice. Both stations have hourly data available over a period of about 50 years (from 1-1-1971 to 1-1-2020).

The correlation between the two data sets is measured with the Pearson correlation coefficient (Pearson, 1895), which can range from -1 (perfect negative linear correlation) to 1 (perfect positive linear correlation). Independent variables will have a value close to zero, though the inverse is not necessarily true.

$$\rho_{h_S, U_{10}} = \frac{\text{cov}(h_S, U_{10})}{\sigma_{h_S} \sigma_{U_{10}}} \quad (23)$$

The wind and water data have a positive correlation of 0.158, which is relatively low. Independence of the two parameters is therefore assumed in this case study, though to improve accuracy a correlated copula could be implemented to better represent the historical conditions. Figure 11 shows histograms of two variables along with their fitted probability density functions. Based on a least squares analysis a lognormal distribution is found with $\sigma = 0.35$ [-], $\mu = -3.06$ m/s, and $\alpha = 8.34$ m/s:

$$f(U_{10}) = \frac{1}{(U_{10} - \mu) \cdot \sqrt{2\pi\sigma^2}} e^{-\frac{\log(\frac{U_{10}-\mu}{\alpha})^2}{2\sigma^2}} \quad (24)$$

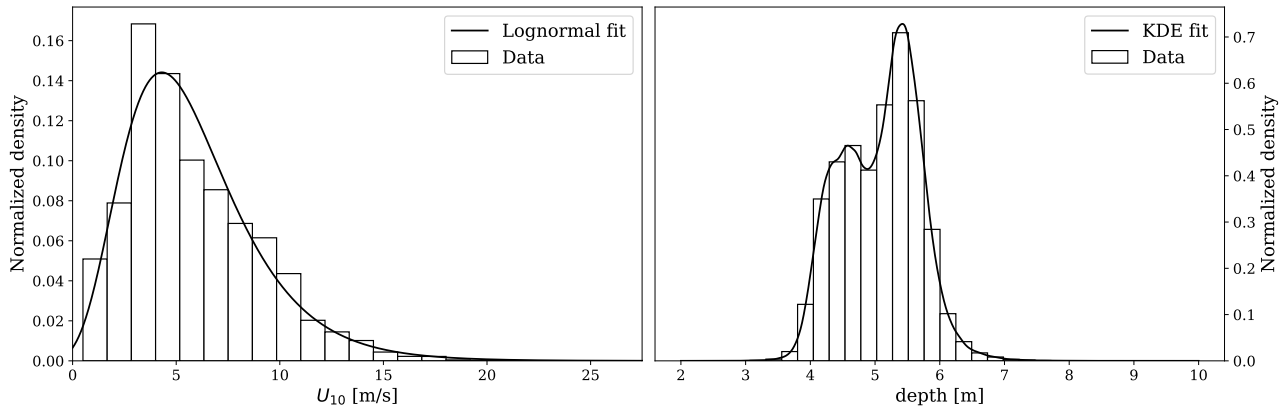


Figure 11: Fitted distributions of historical data for h_S and U_{10}

The bi-modal shape of the water level distribution caused by the influence of the tides makes a standard distribution fit unsuitable. The water level is therefore modelled by a non-parametric Gaussian Kernel Density Estimate (KDE). Next, the KDE of the water level data is combined with the sea level rise probability distribution according to the method described in paragraph 4.1. A climate change scenario of +1 m sea level rise by 2100 is considered, which is the recommended design value according to Klein Tank et al. (2014) for structures along the Dutch coast. It will be modelled as a uniform distribution. The two input distributions and the resulting convoluted distribution are plotted in Figure 14.

By applying the previously presented discretisation procedure in total 4480 load cases are obtained. Filtering out the irrelevant load cases based on their probability of occurrence and expected maximum wave height according to Equations 20 and 21 reduces the amount of load cases by 66% to 1483. Figure 12 shows a visualisation of the filtered and remaining load cases.

Table 2: Probabilistic variables used in the case study

Parameter	Symbol	Distribution	Distribution parameters	Unit
Impact peak duration	τ	Triangular	$a = 5; b = 200; c = 75$	ms
Wind velocity	U_{10}	Lognormal	$\sigma = 0.35; \mu = -3.06; \alpha = 8.34$	m/s
Water level measurements	h_s	KDE	Non-parametric fit of data	m
Sea level rise	h_{SLR}	Uniform	$0 \leq h_{SLR} \leq 1$	m
Surface elevation phase shift (per harmonic i)	ϕ_i	Uniform	$0 \leq \phi_i \leq 2\pi$	rad

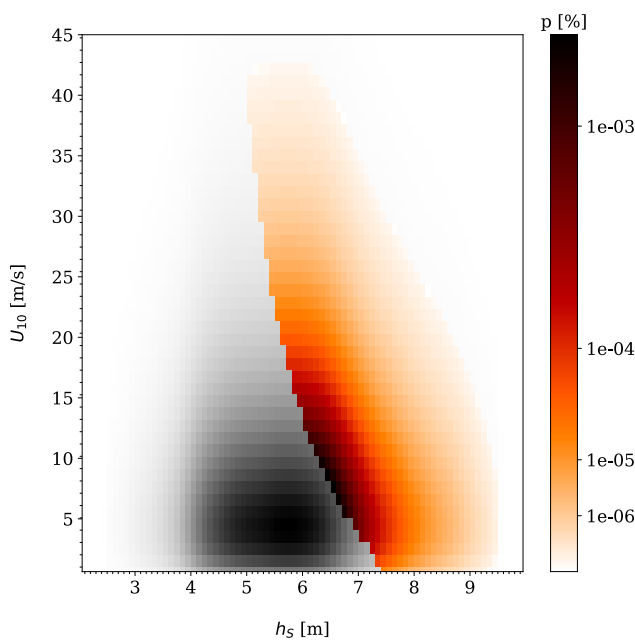


Figure 12: Grid of all load cases, coloured based on probability of occurrence. The greyscale load cases were filtered out based on frequency and/or intensity.

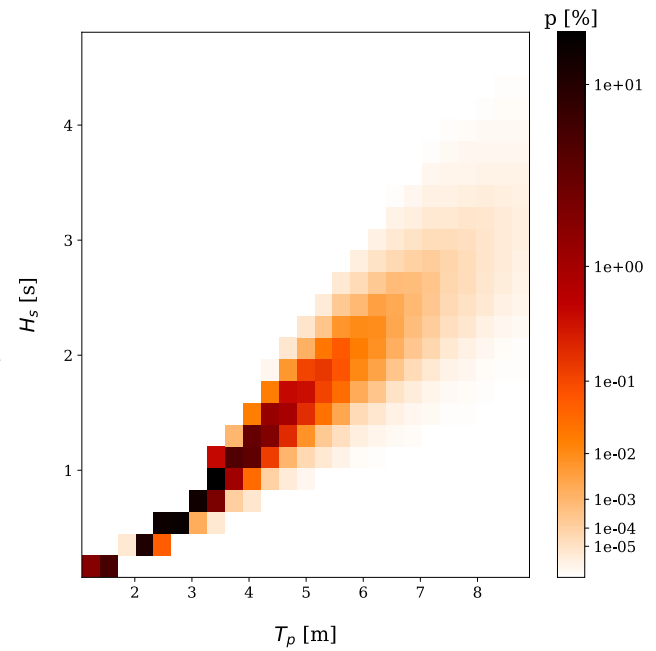


Figure 13: Significant wave height and peak period corresponding to the remaining load cases.

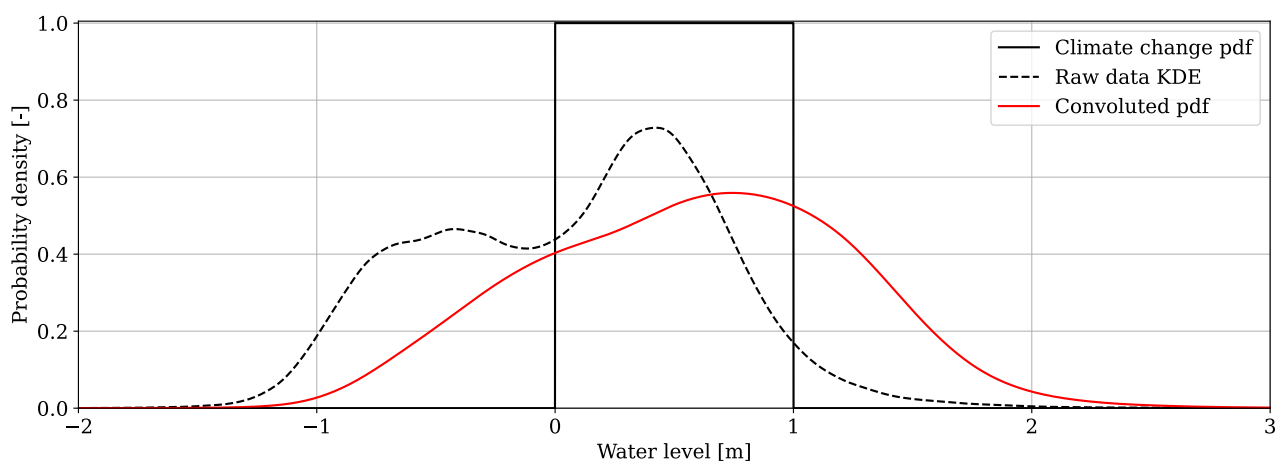


Figure 14: Probability density functions of the water level data, a climate change scenario with +1 m sea level rise, and their combined values.

5.2 Fatigue damage distribution

Before proceeding with the lifetime fatigue analysis, the fatigue damage distribution across the gate and the influence of different modes on the final result is discussed. Besides gaining insight in how the structure behaves, identifying which parts of the gate are most strongly affected by fatigue also makes it possible to limit the lifetime fatigue analysis to points of interest rather than the entire surface.

Applying a random hour-long load case to the gate results in a fatigue distribution as shown in Figure 15. Due to the asymmetric wave impact shape, the fatigue damage is concentrated at the top and bottom of the middle of the gate. The highest fatigue occurs at coordinate P1($x = 5m; y = 0.65m; z = 7.5m$). The overall distribution suggests a high mobilisation of the second mode from Figure 10.

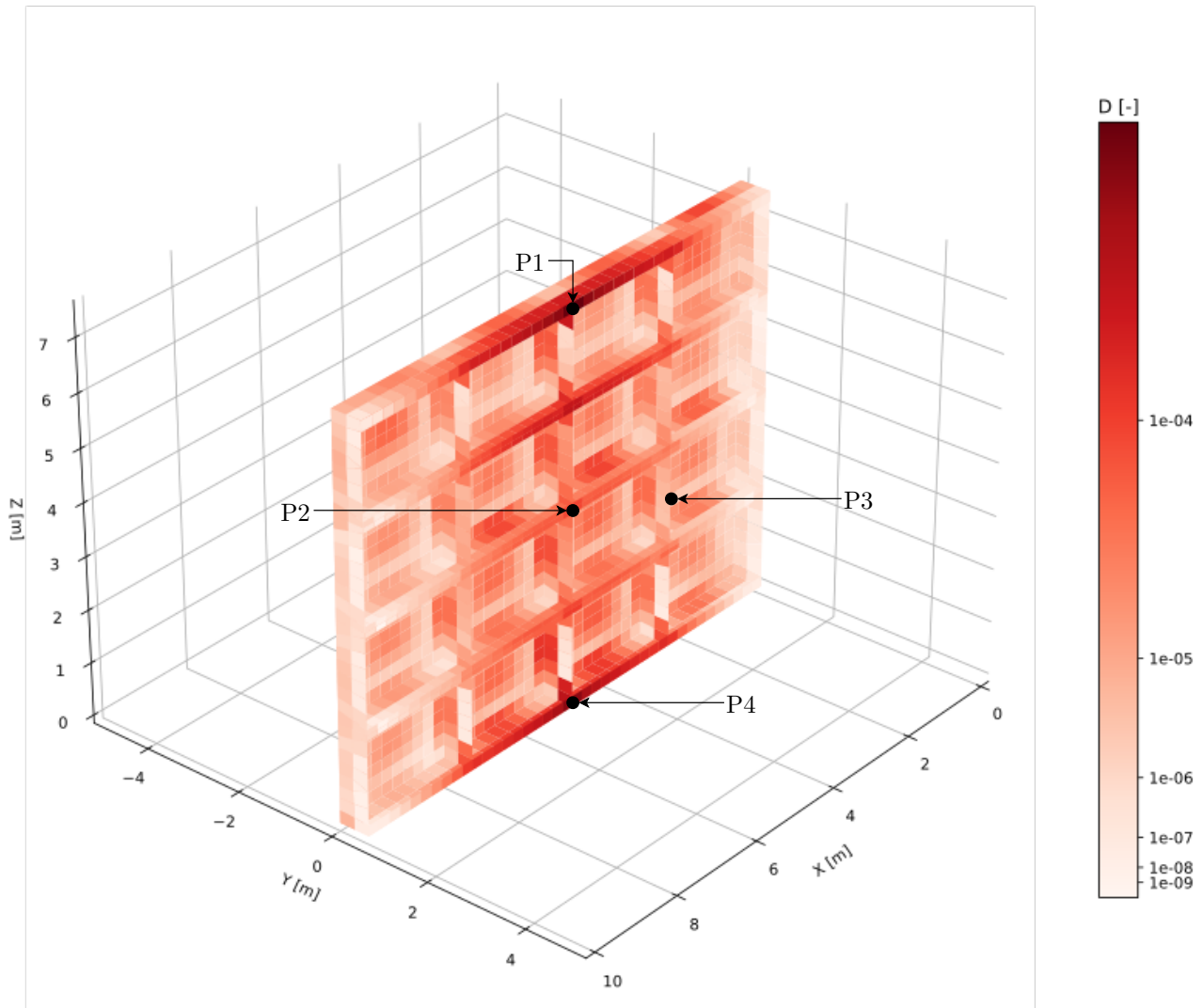


Figure 15: D over the surface of the gate after a hour-long load event with $U_{10} = 30$ m/s, $h_S = 7.5$ m, and $h_L = 4$ m. Points of interest are indicated.

Figure 16 shows the relative importance of each mode in the fatigue damage at four points of interest in the gate. The locations of these points were indicated in Figure 15. Due to the non-linear relation between stress cycles and fatigue damage, which is logarithmic and includes a cut-off limit, it is not possible to simply simulate the fatigue damage caused by each individual mode. Instead, the ratio R was introduced to measure the relative importance of each mode on the total fatigue damage in each coordinate:

$$R = \frac{D_a - D_{a-m}}{D_a} \quad (25)$$

Here, D_a is the fatigue damage factor for a simulation with a modes. D_{a-m} is the fatigue damage factor for the same simulation excluding the response of mode m . Due to the non-linearity of fatigue damage these percentages will not add up to 100%.

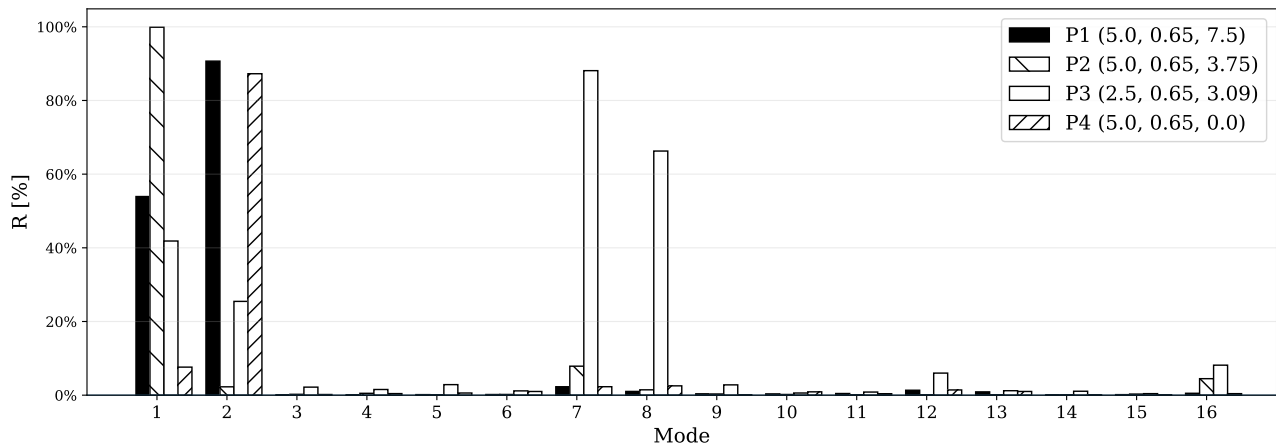


Figure 16: Relative importance of the first 16 modes for the fatigue damage at four notable locations.

The coordinate P1 (5, -0.65, 7.5) was found to be the most heavily loaded part of the gate. The contribution of the second mode is dominant here. The second coordinate, P2 (5, -0.65, 3.75) is located at the centre of the gate. The second mode does not cause significant stresses at this location; virtually all the fatigue damage follows from the first mode. Fatigue damage at coordinate P3 (2.5, -0.65, 3) is dominated by higher modes, especially the seventh and eighth. Finally, P4 (5, -0.65, 0) is located at the bottom middle of the gate and shows a similar pattern as P1.

This result demonstrates the importance of including more than one vibration mode in fatigue analyses of systems similar to the one considered here. The asymmetric load shape over the height and the excitation frequencies of the wave impacts excite higher modes of the gate. At the governing locations, the fatigue damage is dominated by the first and especially second vibration modes. At other locations higher modes were found to be dominant.

5.3 Lifetime fatigue

Next, the fatigue lifetime analysis described in Section 4 is performed to estimate the fatigue lifetime L_D of the gate. This analysis is focused on the most critical point (P1) of the gate as found in the previous paragraph. A Monte Carlo simulation with 1000 repetitions is performed, in which the 1483 hour-long load cases are randomly sampled based on their probability of occurrence, and cumulatively added until failure occurs. Figure 17 shows the accumulation of fatigue damage over time (left) along with the relative importance of the considered load cases (right). The 5th and 95th lower and upper bound of the simulations have been indicated. The distribution in predicted fatigue lifetime can be read along the horizontal line of 100% fatigue damage. The analysis shows that there is a 95% chance that the fatigue lifetime of the gate exceeds 90 years. Vice versa, in the vertical direction, the graph indicates the cumulative failure probability of the gate after a certain time. The probability that the gate has failed due to fatigue after 90 years is approximately 5% and after 98 years approximately 95%. This could also be translated to a failure probability due to fatigue per year, which is often required for safety assessments of flood gates. A higher number of simulations may be desirable to predict minor yearly failure probabilities.

The bandwidth over the simulations is limited. The uncertainty originating from the random phase-amplitude model and the wave impact duration does not lead to a large bandwidth over the high number of load cases and waves over the lifetime over the structure. Sampling uncertainty does lead to some bandwidth: by chance some lifetime simulations will have more or less high-impact events than on average. However, mainly the more commonly occurring load cases with intermediate wave conditions and a water level at the overhang contribute to the fatigue damage. These high frequency of occurrence events lead to less sampling uncertainty than more rare events. Scenario uncertainties like sea level rise could cause larger bandwidths when included in the analysis.

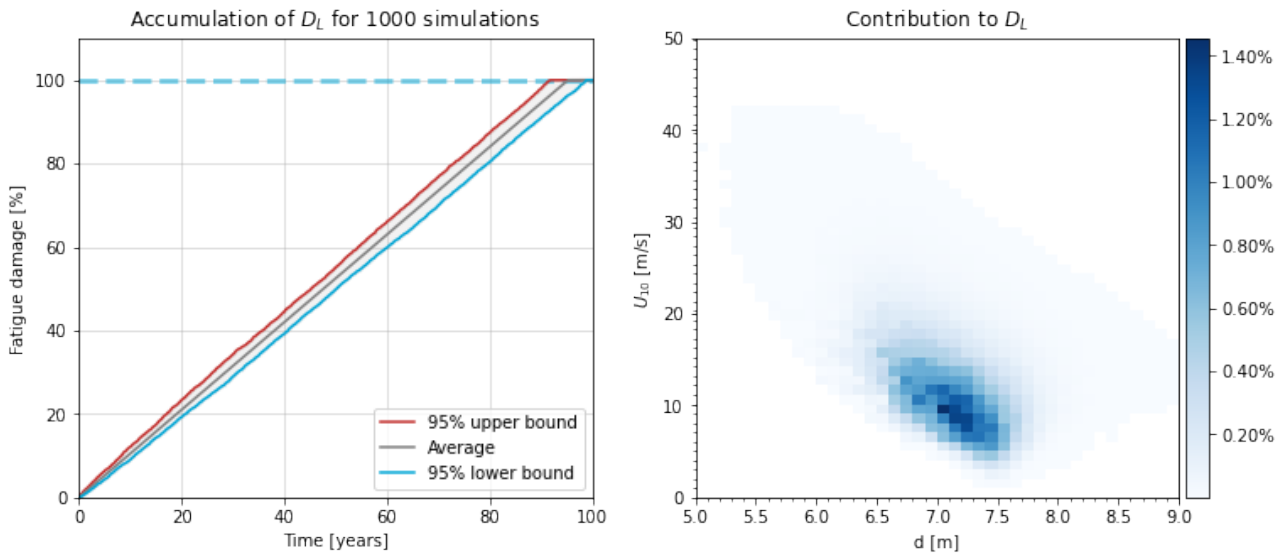


Figure 17: Left: Monte Carlo simulations of fatigue accumulation over time. Right: Percentage of total lifetime fatigue damage D_L caused by each load case.

Figure 17 (right) shows which load cases contributed most to the overall fatigue damage. It stands out that the moderately strong but common load events are much more important than the extreme events. In this case this is likely partly due to the bathymetry of the system which does not allow very large waves to develop.

5.4 Convergence of the solution

Convergence of the solution is discussed both for the number of modes taken into account in the fluid-structure interaction model and the resolution of the load cases considered in the probabilistic fatigue assessment.

5.4.1 Convergence of the fluid-structure response

The fluid-structure interaction response model is based on a coupled modal decomposition of the structure and fluid. This solution is exact for the corresponding theoretical formulation of the problem, which is an infinite summation of modes. However, to numerically evaluate the solution, the number of modes should be truncated to a finite number.

Tsouvalas and Metrikine (2016) provides several standard rules for the number of structural modes to take into account. As a rule of thumb, it is sufficient to include all structural modal shapes corresponding to the eigenfrequencies that are up to twice as high as the maximum response frequency of interest. This frequency is not clear-cut in a probabilistic model such as this one however. Convergence of the results for the number of structural modal shapes has been checked in this study by comparing the contribution of higher modes to the total response. Results have sufficiently converged for this case study when the first 16 structural modal shapes are evaluated.

For the fluid modes, Tsouvalas et al. (2015) apply a convergence criterion which matches the obtained amplitude of the displacement of the gate $w_g(x, z)$ [m] with that of the fluid layer at the surface of the gate $w_f(x, y = 0, z)$ [m]. Here, we use a similar method, where we define the average error between the predicted velocity of the gate and the fluid over the interface surface.

$$\delta_u(f) = \left| \frac{\overline{v_g(x, z, f)} - \overline{v_f(x, y = 0, z, f)}}{\overline{v_g(x, z, f)}} \right| \quad (26)$$

For the convergence test, the system is excited by a single unit peak load with a relatively short duration (0.05 s) so that a large number of modes is excited. The load is only applied in the upper left quadrant of the gate to excite the anti-symmetric modes over the horizontal as well. The amount of structural modes is kept

constant at $k = 16$. The number of fluid modes in the fluid domains in front of the gate are increased from 1 to 225. The results are plotted in Figure 18.

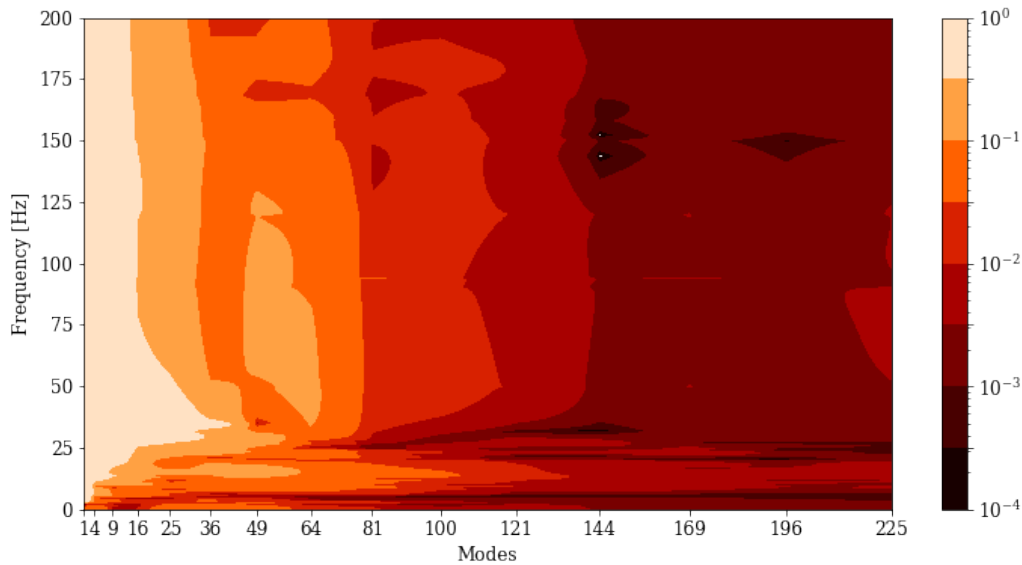


Figure 18: The error $\delta_u(f)$ for 1 to 225 fluid modes at a constant number of 16 structural modes.

Convergence of the results for the number of fluid modes is most critical around a frequency range of 20-25 Hz, where the natural frequencies of several higher modes are concentrated. The average error $\delta_u(f)$ [-] over all the frequencies falls below 10% with 36 fluid modes and below 1% at 121 fluid modes. A number of 100 fluid modes was chosen, which is deemed sufficiently accurate for the purpose of this case study.

5.4.2 Convergence for the load case resolution

The historic data in this case study were discretized with a resolution that resulted in 4480 load cases, of which 1066 were included in the fatigue analysis after filtering. Convergence of the solution for this resolution is checked in by varying the bin size according to the routine presented in paragraph 4.2. Figure 19 shows the standard deviation of the outcome of the fatigue analysis based on random values of h_S and U_{10} in each grid cell versus the chosen representative values.

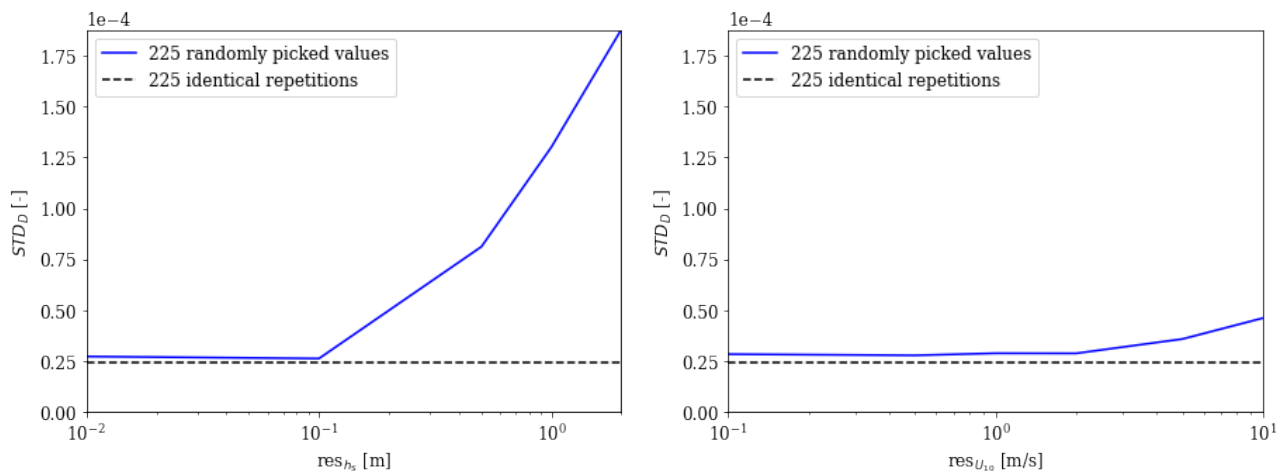


Figure 19: Convergence of resolutions to the inherent variance of the model.

As expected, the standard deviation asymptotically approaches a value above zero for increasing resolutions. That value is the variance caused by the random variables within the model, such as the impact duration and

randomness of the wave field. For resolutions higher than $\Delta_{h_s} = 0.1$ m and $\Delta_{U_{10}} = 1$ the standard deviation of the outcome has converged to this variance. At this point the marginal return in increased accuracy for further narrowing the resolution rapidly diminishes. These resolutions are therefore used in this case study.

5.5 Comparison with methods presently used in engineering practice

Presently in engineering practice, the wave climate over the lifetime of the gate is often characterised by a limited set of design storms with defined return periods and significant wave heights. The frequency of different wave heights within such a storm is derived from (modified) Rayleigh distributions like those described in Battjes and Groenendijk (2000). The structural response to each wave is then evaluated individually. The theory of Kolkman and Jongeling (2007*b,a*) is generally employed for this purpose, which is based on a quasi-static evaluation of the structural stresses. A dynamic amplification factor is then applied to account for dynamic behaviour based on a single degree of freedom (SDOF) representation of the structure. Finally, the fatigue response per individual wave is summed proportional to their probability of occurrence to find the total fatigue damage experienced by the gate during a particular storm.

The presented design method improves on this existing method on several aspects. The response of the structure is explicitly simulated for all load cases relevant to the fatigue lifetime. It is not necessary to simplify the analysis to a limited set of design storms. Furthermore a novel semi-analytical fluid-structure interaction model is employed (Tieleman et al., 2022) to determine the multi-modal dynamic response of the flood gate in water, rather than a SDOF representation. The following paragraphs investigate the effect of the two above mentioned aspects of the presented design method based on the parameters defined in the case study.

5.5.1 Consecutive versus individual waves

To investigate the effect of interfering vibrations due to consecutive wave impacts, a comparison will be made between two approaches. First, a random wave state is generated and the individual wave impacts are identified. The sequence of impact velocities is then used to evaluate the response to each impact individually. The structural response to the individual waves will be allowed to fully damp out. In the second analysis the response is derived for the full (identical) time series following the method described in this paper. Quasi-steady wave fluctuations are ignored in both cases. The fatigue damage of all the isolated waves is summed up and compared to the fatigue damage caused by the time series with consecutive waves. Figure 20 gives an example of the structural response of the gate for both analyses.

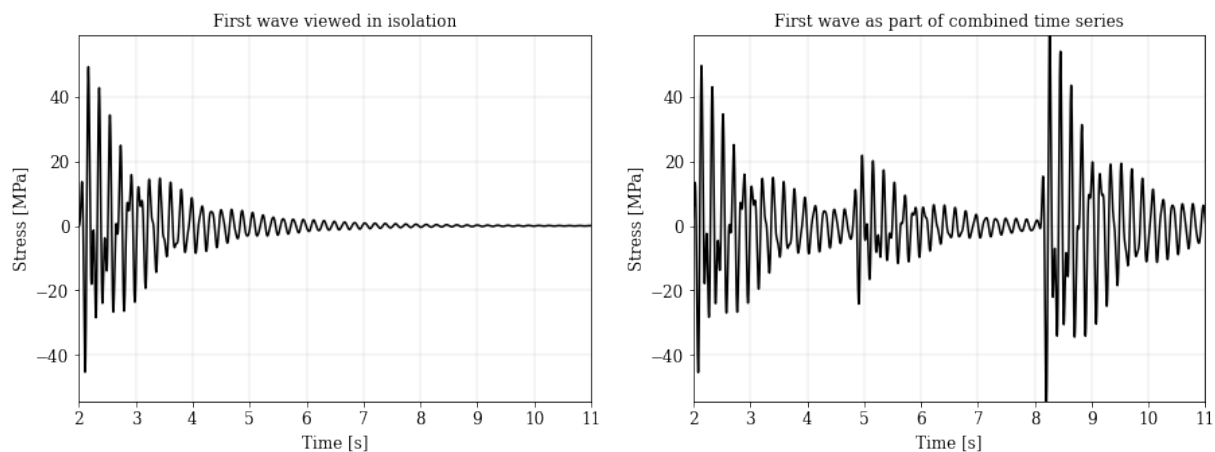


Figure 20: The stress response of the gate when a wave is isolated and allowed to damp out vs. the response to the full time series.

In the long term, vibrations due to consecutive waves should reinforce and cancel each other out equally often due to their random phase. However, because fatigue damage is logarithmic rather than linearly proportional to the magnitude of stress variations, this does not mean that the impact on the fatigue of the gate will be averaged out as well. The increased fatigue damage from constructively interfering vibrations is larger than the decrease in fatigue due to destructively interfering vibrations.

The effect is stronger when waves follow each other in short succession, where the vibrating gate does not have the time to damp out before the next wave arrives. This suggests a dependence on the mean water level, because if the mean water level h_S is equal to the overhang height h_G virtually every wave will cause an impact. In contrast, wave impacts will be more sporadic when the mean water level is significantly lower. To account for this effect the comparison is repeated for different combinations of environmental conditions. Table 3 shows the ratio D_{iso}/D_{full} , where D_{iso} is the predicted fatigue damage by modelling isolated waves and D_{full} the fatigue damage resulting from the entire time series with consecutive wave impacts.

Table 3: Average D_{iso}/D_{full} of 15 repetitions for various environmental conditions. The empty cells represent cases where all stress cycles fall below the cut-off limit.

U_{10} [m/s]	h_S [m]						
	$h_G-1.5$	h_G-1	$h_G-0.5$	h_G	$h_G+0.5$	h_G+1	$h_G+1.5$
10	-	82%	81%	78%	79%	82%	-
40	84%	84%	83%	83%	83%	84%	84%

From these results, it follows that the effect of waves reinforcing each other can be very significant. On average the fatigue damage is underestimated by about 18% in these simulations when regarding the response to individual waves. Fatigue analyses of similar systems which regard each wave in isolation therefore risk underestimating the fatigue damage of the structure.

The relative error is slightly higher for lower wind velocities, as these lead to wave spectrum with shorter wave periods and thus less time for vibrations to damp out in between wave impacts. The water level may have some influence on the fluid damping due to surface waves and compressibility. However, this type of damping is usually insignificant for the water levels and vibration frequencies involved with these types of problems as was discussed in Tieleman et al. (2019a). The relative error therefore shows no clear dependence on the water level.

A relatively high isotropic damping factor ($\eta = 0.02$) was applied in this study. For cases with lower isotropic damping factors the effect of interference due to consecutive impacts is likely to be stronger.

5.5.2 Multiple versus single degree of freedom response model

The theory of Kolkman and Jongeling (2007b,a) is often employed in practice to determine the response of flood gates for wave impacts. A key element of this approach is that the structural stress distribution over the gate is predicted quasi-statically for the wave impact peak load. A dynamic amplification factor (DAF) is then applied to this stress field to correct for the dynamic behaviour of the structure. This amplification factor is based on a single degree of freedom (SDOF) representation of the structure, whereas the model routine presented in this paper is multiple degree of freedom (MDOF). Hydrodynamic coefficients or non-dimensionalised added virtual mass incremental factors (Kwak and Kim, 1991; Kwak, 1996) are applied to account for the influence of the fluid.

Several variants of this approach exist. In some cases, only one stress cycle per wave impact is accounted for. The DAF then is a constant for each impact. More advanced analyses do take into account multiple vibrations after each impact by applying a time-varying DAF based on the time response of the single degree of freedom system after each impact.

In this analysis, the DAF approach is approximated as follows. First, the full semi-analytical model is used to determine the normalised quasi-static response of the gate to a wave impact peak load. This results in a set of modal coefficients of the gate $A_{k,qs}$ and distributions for each directional stress component $\sigma_{qs,jj}$. Then, the semi-analytical fluid-structure interaction model is applied with only a single structural modal shape to predict the response for a random hour-long load case. The model implicitly includes the hydrodynamic response. This is the same as applying relatively precisely determined hydrodynamic coefficients. This results in a single time domain response signal in terms of the modal coefficient $A_{1,dyn}(t)$. The DAF is then determined by:

$$\text{DAF}(t) = \frac{A_{1,dyn}(t)}{A_{1,qs}} \quad (27)$$

and subsequently applied to the stress fields corresponding to the quasi-static response as follows:

$$\sigma_{\text{DAF},jj}(t) = \text{DAF}(t) \cdot \sigma_{qs,jj} \quad (28)$$

The results of the presented design method are compared to this DAF approach. Quasi-steady wave fluctuations are again ignored. The analysis is performed using the DAF approach both for individual and consecutive waves (see paragraph 5.5.1). Based on Figure 16, it is expected that a DAF approach based on a single degree of freedom representation of the structure will significantly distort the fatigue damage. Table 4 shows the fatigue damage predicted by the semi-analytic approach presented in this paper D_{SA} (which takes higher modes into account), and the fatigue damage predicted by the DAF approach D_{DAF} (for both consecutive and individually evaluated waves). The locations on the gate correspond to those defined in paragraph 5.2.

Table 4: Fatigue damage at points of interest on the gate for different methods. Normalised to MDOF results.

Model approach	P1 (5, -0.65, 7.5)	P2 (5, -0.65, 3.75)	P3 (2.5, -0.65, 3)	P4 (5, -0.65, 0)
MDOF (consecutive waves)	100%	100%	100%	100%
DAF (consecutive waves)	121%	147%	0%	0.1%
DAF (individual waves)	111%	133%	0%	0.05%

The DAF approach predicts more fatigue damage at the critical point P1 at the top of the gate and the centre of the gate (P2). Because the quasi-static response to a confined wave impact mainly affects the top middle of the gate, this approach concentrates all energy in this area (See Figure 21). Conversely, this different distribution means that the stresses predicted by the DAF method in points P3 and P4 fall almost entirely below the cut-off limit and therefore barely cause any fatigue damage. The presented design method does predict fatigue damage for location P3 en P4 dominated by the seventh and second mode respectively. The difference at P4 is especially noteworthy, as Figure 15 demonstrates that significant fatigue will occur here due to second-mode vibrations. For comparison, Figure 21 shows the fatigue damage over the entire gate for the DAF approach. The fatigue damage predicted the DAF approach roughly follows the shape of the wave impact pressure over the height, while the fatigue damage predicted by the presented design method is governed by the actual dynamic behaviour of the gate.

Combining the DAF approach with the effect of considering all waves in isolation (as in paragraph 5.5.1) follows the same pattern, but underestimates the response everywhere by omitting the influence of wave reinforcement.

6 Discussion

Several key assumptions and potential improvements of the presented design method are discussed in this section. First of all, all waves were considered to approach the flood gate perpendicularly in this study. Perpendicular waves lead to the highest wave impact loads. Accounting for non-perpendicular waves therefore would result in lower overall forces on the gate. However, the resulting loads are non-uniformly distributed over the width of the gate and will therefore excite anti-symmetric modes. This may result in local stress concentrations that differ from the case with perpendicular waves. The response model is fully capable of predicting the response to uniform wave loads. Given a suitable theory to predict non-uniform wave impact loads, the model routine can therefore be adapted relatively straightforwardly to include non-perpendicular waves. For example, De Almeida and Hofland (2021) describe the effects of oblique wave attack in a flume.

Furthermore, a linear wave theory was applied in this paper to predict the surface elevation time series and resulting wave impact velocities and quasi-steady wave pressures. Especially in shallow waters, waves exhibit non-linear behaviour with steeper peaks and flatter troughs. This leads on average to higher wave impact velocities and thus a shorter fatigue life than what would be predicted based on linear wave theory. To increase the applicability range of the design method, a higher wave order theory could be applied relatively straightforward within the model routine. Sobey (2009) proposes analytical solutions up to the fifth order. However, based on criteria from Hedges (1995), De Almeida and Hofland (2020b) found that for the largest impacts around the waterline the impact velocities obtained from linear wave theory match non-linear theory well.

Another source of non-linearity can be the presence of entrapped air under the overhang during wave impacts. This may effectively lead to longer impact durations. Research on this topic is ongoing based on the experimental results from De Almeida et al. (2019); De Almeida and Hofland (2020b). Possible ways of accounting for this in the model include adding the air as a separate domain, or modelling the overhang with a certain spring stiffness. On a related note, an effective measure to reduce impact pressures is the application of a ventilation hole.

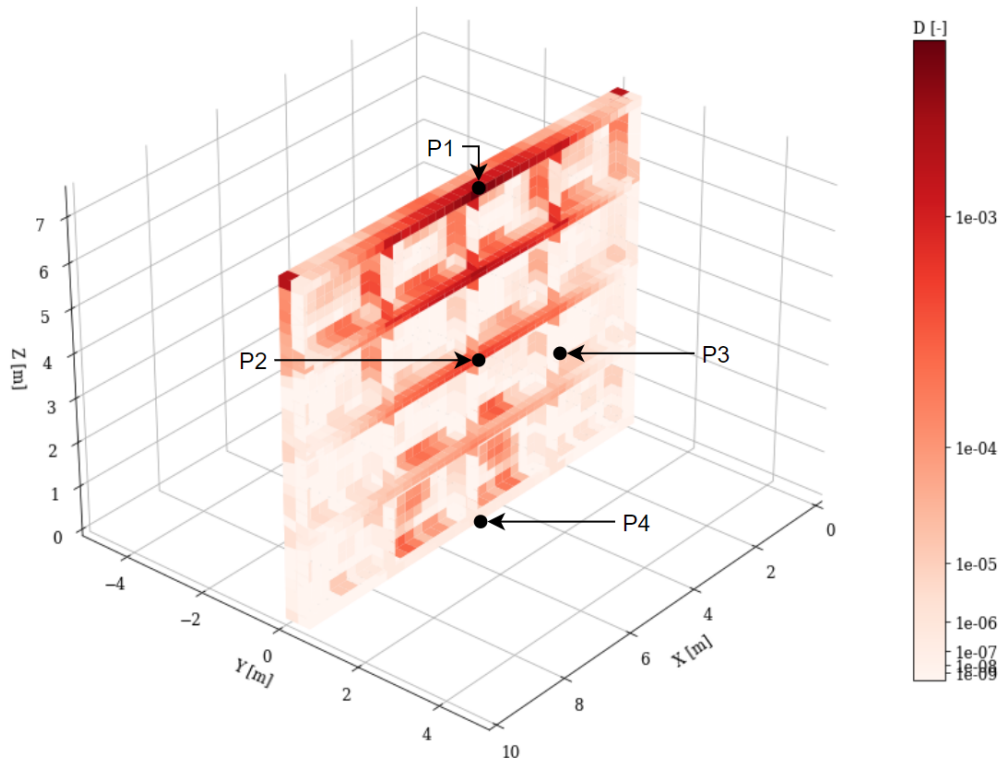


Figure 21: D_{DAF} over the surface of the gate after a hour-long load event with $U_{10} = 35$ m/s, $h_S = 7.5$ m, and $h_L = 4$ m. Points of interest indicated.

Hofland et al. (2019) showed how this measure can be included in the model to predict impulsive impact pressures. Such a measure would also reduce the presence of air under the overhang during an impact.

Air bubbles in the water column also have an effect on the fluid response to the gate motion. Air bubbles can significantly decrease the sound velocity in the water in front of the gate (Bullock et al., 2007). The sound velocity of water is around $c_p = 1500$ m/s, but could drop as low as 150 m/s for a water-air mixture with 1% air (Gibson, 1970). This may lead to lower resonance frequencies of the fluid due to compressibility and therefore alter the fluid response. Acoustic damping may become more significant as well. Trial runs for the extreme case where $c_p = 150$ m/s suggest the fatigue damage could decrease as much as 50%. To investigate the actual effect on the fatigue assessment a sensitivity analysis could be performed for various levels of air bubbles, and thus sound velocities, extending over various distances from the gate. The dependence between wave properties and air entrapment could also influence the impact duration. Research on this topic based on the results by De Almeida and Hofland (2021) is still ongoing.

The probability density function of the mean water level and wind velocity have been derived with basic curve fitting methods, as this is not the main focus of this study. A relatively straightforward improvement would be to evaluate the correlation in the upper tail of the probability density function separately, because rare high-impact events are more likely to be correlated than day-to-day water depth and wave statistics. This correlation would likely lead to the prediction of a slightly lower fatigue lifetime, although the fatigue was found to mainly depend on frequent loads. The taken approach is thus conservative. Additionally, a more rigorous estimate based on climate modelling and an improved wave transformation computation based on a realistic bathymetry such as by Groeneweg et al. (2009) is recommended for application in more advanced design stages.

Finally it is noted that although this study focuses on confined wave impacts on an overhang, the presented design method may also be applied for example to breaking wave impacts. An alternative model should then be applied to predict the impulsive part of the wave load. Such theoretical models do exist for breaking wave impacts (Bagnold, 1939; Minikin, 1950; Takashi, 1994; Oumeraci et al., 2001; Cuomo et al., 2010).

7 Conclusions

A novel probabilistic design method has been presented that can efficiently and accurately determine the expected fatigue lifetime of a flood gate subjected to confined dynamic wave impacts. The design method takes into account the entire joint probability function of the wind velocity and mean water level based on historical data including an adjustment for sea level rise. This probability function is then translated to a set of discrete load cases and an associated probability of occurrence. A method was suggested to determine the optimal size of this discretization by minimising the internal variance of each interval. Impulse theory is used to predict the wave impact pressures for each load case. A novel semi-analytical fluid-structure interaction model is employed to predict the dynamic response of the flood gate. The computational efficiency of this semi-analytical model facilitates a much larger number of simulations compared to numerical alternatives. The applied model routine is modular and therefore adaptable to many different situations.

The presented design method has been applied to a case study inspired by the situation of the Afsluitdijk in the Netherlands. It was demonstrated that the method is effective in assessing the fatigue accumulation over the lifetime of the gate. For the investigated case with a shallow sea, the mid-sized but common load events were shown to contribute more to the fatigue lifetime than rare events. Furthermore, the non-uniform pressure distribution and excitation frequencies of the wave impacts result in significant higher mode vibrations of the gate. A breakdown of the contribution of the different response modes showed that higher modes have a high contribution to the fatigue damage in many areas of the gate, including the governing location.

The outcome of the presented method was compared to the dynamic amplification factor (DAF) approach presently used in practice. The DAF approach is based on a single degree of freedom representation of the structure and usually regards the response to individual waves rather than consecutive waves in a design storm. It was shown that the existing design method does not accurately predict the distribution of fatigue damage of the gate. At some points this caused an overestimation of the stresses, while at others it lead to a significant underestimation of the critical fatigue load. This shows that the DAF approach is questionable when the gate response shows a clear participation of higher eigenmodes. Moreover, neglecting the reinforcement effect of vibrations caused by consecutive waves leads to an underestimation of the fatigue damage. The design method presented in this paper is therefore a significant improvement on existing methods in terms of accuracy, without compromising on computational efficiency.

Acknowledgements

This work was funded by NWO, Netherlands grant ALWTW.2016.041. We thank Witteveen+Bos for providing the time, resources, and knowledge that made this paper possible.

Notations

Name	Symbol	Unit
Acceleration due to gravity	g	m/s^2
Wind velocity at 10m+MSL	U_{10}	m/s
Sea water level	h_s	m
Lake water depth	h_L	m
Sea level rise	h_{SLR}	m
Gate height	h_G	m
Wave length	L_w	m
Overhang length	L_y	m
Gate width	W	m
Gate deflection	$w(x, z)$	m
Wind fetch	F	m
Reflection coefficient	c_r	-
Wave impact duration	τ	s
Steel density	ρ_s	kg/m^3
Water density	ρ_w	kg/m^3
Young's modulus of steel	E_s	MPa
Damping ratio	ζ	-
Fatigue damage	D	-
Fatigue lifetime	L_D	years
Frequency	f	Hz
Variance density	$E(f)$	m^2/Hz
n^{th} spectral moment	m_n	m^2
Compressibility correction factor	β_{im}	-
Wave impact velocity	U_w	m/s
Significant wave height	H_{m0}	m
Pressure field	$p(x, z)$	Pa
Spectral peak wave period	T_{m02}	s
Damping factor	η	-
Gate mass	M_G	kg
Detail category	$\Delta\sigma_c$	MPa
Thickness	t	m
Mean error	$\delta_u(f)$	-

References

- Airy, G.B. (1845). On tides and waves. *Encyclopaedia Metropolitana*, **5**.
- Bagnold, R. and Ramkema, C. (1978). A model law for wave impacts on coastal structures. *Proceedings of the International Conference on Coastal Engineering*, **16**(Figure 7), 2308–2327.
- Bagnold, R.A. (1939). Interim Report on Wave-Pressure Research. Technical Report 7, Institution of Civil Engineers. doi:10.1680/ijoti.1939.14539.
- Battjes, J.A. and Groenendijk, H.W. (2000). Wave height distributions on shallow foreshores. *Coastal engineering*, **40**(3), 161–182.
- Benasciutti, D. and Tovo, R. (2006). Comparison of spectral methods for fatigue analysis of broad-band Gaussian random processes. *Probabilistic Engineering Mechanics*, **21**(4), 287–299. ISSN 02668920. doi:10.1016/j.probengmech.2005.10.003.
- Bretschneider, C.L. (1959). *Wave variability and wave spectra for wind-generated gravity waves*. 118. The Board.
- Bullock, G., Obhrai, C., Peregrine, D. and Bredmose, H. (2007). Violent breaking wave impacts. part 1: Results from large-scale regular wave tests on vertical and sloping walls. *Coastal Engineering*, **54**(8), 602–617. doi:https://doi.org/10.1016/j.coastaleng.2006.12.002.
- CEN (2012). *Eurocode 3: Design of Steel Structures - Part 1-9: Fatigue*. CEN.
- Chen, X., Hofland, B., Molenaar, W., Capel, A. and Van Gent, M.R. (2019). Use of impulses to determine the reaction force of a hydraulic structure with an overhang due to wave impact. *Coastal Engineering*, **147**, 75–88.
- Cuomo, G. (2007). Wave impacts on vertical seawalls and caisson breakwaters. *PIANC magazine "on course"*, **127**.
- Cuomo, G., Allsop, W., Bruce, T. and Pearson, J. (2010). Breaking wave loads at vertical seawalls and breakwaters. *Coastal Engineering*, **57**(4), 424–439. ISSN 03783839. doi:10.1016/j.coastaleng.2009.11.005.
- De Almeida, E. and Hofland, B. (2020a). Experimental Observations on Impact Velocity and Entrapped Air for Standing Wave Impacts on Vertical Hydraulic Structures with Overhangs. *Journal of Marine Science and Engineering*, **8**(11), 857. ISSN 2077-1312. doi:10.3390/jmse8110857.
- De Almeida, E. and Hofland, B. (2020b). Validation of pressure-impulse theory for standing wave impact loading on vertical hydraulic structures with short overhangs. *Coastal Engineering*, **159**. doi:10.1016/j.coastaleng.2020.103702.
- De Almeida, E. and Hofland, B. (2021). Standing wave impacts on vertical hydraulic structures with overhangs for varying wave fields and configurations. *Journal of Coastal and Hydraulic Structures*, **1**, 1–24. doi:10.48438/jchs.2021.0010.
- De Almeida, E., Hofland, B. and Jonkman, S.N. (2019). Wave Impact Pressure-Impulse on Vertical Structures with Overhangs. *Coastal Structures*, 86–96. doi:10.18451/978-3-939230-64-9_010.
- Downing, S. and Socie, D. (1982). Simple rainflow counting algorithms. *International Journal of Fatigue*, **4**(1), 31–40. ISSN 01421123. doi:10.1016/0142-1123(82)90018-4.
- Gibson, F.W. (1970). Measurement of the effect of air bubbles on the speed of sound in water. *The journal of the Acoustical Society of America*, **48**(5B), 1195–1197.
- Groeneweg, J., Geerse, C., Gautier, C., van Haaren, D., Camarena Calderon, A. and Vuik, V. (2013). Hydraulische randvoorwaarden voor het ontwerp van de versterking van de afsluitdijk. Technical Report 1207150-000-HYE-0009, Deltares.
- Groeneweg, J., van der Westhuysen, A., van Vledder, G., Jacobse, S., Lanssen, J. and van Dongeren, A. (2009). Wave modelling in a tidal inlet: performance of SWAN in the wadden sea. *Proceedings Of The 31st International Conference on Coastal Engineering*, 411–423.

- Hasselmann, K., Barnett, T., Bouws, E., Carlson, H., Cartwright, D., Enke, K., Ewing, J., Gienapp, H., Hasselmann, D., Kruseman, P., Meerburg, A., Muller, P., Olbers, D., Richter, K., Sell, W. and Walden, H. (1973). Measurements of wind-wave growth and swell decay during the joint north sea wave project (jonswap). *Deut. Hydrogr. Z.*, **8**, 1–95.
doi:<http://resolver.tudelft.nl/uuid:f204e188-13b9-49d8-a6dc-4fb7c20562fc>.
- Hedges, T. (1995). Regions of validity of analytical wave theories. *Proceedings of the Institution of Civil Engineers-Water Maritime and Energy*, **112**(2), 111–114. doi:<https://doi.org/10.1680/iwtme.1995.27656>.
- Hofland, B., Kaminski, M. and Wolters, G. (2010). Large Scale Wave Impacts on a Vertical Wall. *Coastal Engineering Proceedings*, **1**(32), 15. ISSN 2156-1028. doi:10.9753/icce.v32.structures.15.
- Hofland, B., Passos, M. and De Almeida, E. (2019). Effect of venting holes to relieve wave impact pressures on flood gates with overhangs. *Proceedings of Coastal Structures 2019*, 190–199.
doi:10.18451/978-3-939230-64-9_020.
- Holthuijsen, L.H. (2007). *Waves in Oceanic and Coastal Waters*, volume 4. Cambridge University Press, Cambridge. ISBN 9780511618536. doi:10.1017/CBO9780511618536.
- Hughes, S.A. (1984). The TMA shallow-water spectrum description and applications. Technical Report CERC-84-7, Coastal Engineering Research Center (US). doi:<http://hdl.handle.net/11681/12522>.
- Hurk, B.J.J.M., Tank, A.K., Lenderink, G., van Ulden, A., van Oldenborgh, G.J., Katsman, C., van den Brink, H., Keller, F., Bessembinder, J., Burgers, G. et al. (2006). *KNMI climate change scenarios 2006 for the Netherlands*. KNMI.
- Klein Tank, A., Beersma, J., Bessembinder, J., Van den Hurk, B. and Lenderink, G. (2014). *KNMI 14: Klimaatscenario's voor Nederland*. KNMI.
- KNMI (2020). Daily historical weather data of the netherlands.
<http://projects.knmi.nl/klimatologie/daggegevens/selectie.cgi>. Data retrieved in October 2020.
- Kolkman, P.A. and Jongeling, T.H.G. (2007b). *Dynamic behaviour of hydraulic structures - Part A*. WL — Delft Hydraulics.
- Kolkman, P.A. and Jongeling, T.H.G. (2007a). *Dynamic behaviour of hydraulic structures - Part B*. WL — Delft Hydraulics.
- Kortenhaus, A., Oumeraci, H., Allsop, N., McConnell, K., Van Gelder, P., Hewson, P., Walkden, M., Müller, G., Calabrese, M. and Vicinanza, D. (1999). Wave impact loads-pressures and forces. *Final Proceedings, MAST III, PROVERBS-Project, IIa: Hydrodynamic Aspects*.
- Kwak, M.K. (1996). Hydroelastic Vibration of Rectangular Plates. *Journal of Applied Mechanics*, **63**(1), 110. ISSN 00218936. doi:10.1115/1.2787184.
- Kwak, M.K. and Kim, K.C. (1991). Axisymmetric vibration of circular plates in contact with fluid. *Journal of Sound and Vibration*, **146**(3), 381–389. ISSN 10958568. doi:10.1016/0022-460X(91)90696-H.
- Leblond, C., Sigrist, J., Auvity, B. and Peerhossaini, H. (2009). A semi-analytical approach to the study of an elastic circular cylinder confined in a cylindrical fluid domain subjected to small-amplitude transient motions. *Journal of Fluids and Structures*, **25**(1), 134–154. ISSN 08899746.
doi:10.1016/j.jfluidstructs.2008.04.004.
- Matsuishi, M. and Endo, T. (1968). Fatigue of metals subjected to varying stress. *Japan Society of Mechanical Engineers, Fukuoka, Japan*, **68**(2), 37–40.
- Miner, M. (1945). Cumulative fatigue damage. *Journal of Applied Mechanics*, **12**(3), A159–A164.
- Minikin, R. (1950). *Winds, Waves, and Maritime Structures: Studies in Harbour Making and in the Protection of Coasts*. Griffin. ISBN 50013644.
- Newland, D.E. (2012). *An introduction to random vibrations, spectral & wavelet analysis*. Courier Corporation. ISBN: 9780582215849.

- Oumeraci, H., Kortenhaus, A., Allsop, W., De Groot, M., Courch, R., Vrijling, H. and Voortman, H. (2001). *Probabilistic Design Tools for Vertical Breakwater*. CRC Press. ISBN 978-9058092496.
- Pearson, K. (1895). Notes on regression and inheritance in the case of two parents. *Proceedings of the Royal Society of London*, **58**, 240–242.
- Rijkswaterstaat (2020a). Project overview Afsluitdijk. <https://www.rijkswaterstaat.nl/water/projectenoverzicht/afsluitdijk>.
- Rijkswaterstaat (2020b). Rijkswaterstaat waterinfo. <https://waterinfo.rws.nl/>. Data retrieved in October 2020.
- Rychlik, I. (1993). On the ‘narrow-band’ approximation for expected fatigue damage. *Probabilistic Engineering Mechanics*, **8**(1), 1–4. ISSN 02668920. doi:10.1016/0266-8920(93)90024-P.
- Sobey, R.J. (2009). Analytical solutions for steep standing waves. *Proceedings of the Institution of Civil Engineers-Engineering and Computational Mechanics*, **162**(4), 185–197.
- Takashi, S. (1994). A proposal of impulsive pressure coefficient for design of composite breakwater. In: *Proceedings of the International Conference on Hydrotechnical Engineering for Port and Harbor Construction*, 489–504.
- Tieleman, O.C. (2016). *The dynamic behaviour of pump gates in the Afsluitdijk*. Master’s thesis, Delft University of Technology. doi:http://resolver.tudelft.nl/uuid:d68f9483-e374-4c38-ace3-89594e38daf0.
- Tieleman, O.C., Hofland, B. and Jonkman, S.N. (2018). Bending Vibrations of the Afsluitdijk Gates Subjected to Wave Impacts: A Comparison of Two Design Methods. In: *Proceedings of the 34th PIANC World Congress*.
- Tieleman, O.C., Hofland, B., Tsouvalas, A., De Almeida, E. and Jonkman, S.N. (2021). A fluid–structure interaction model for assessing the safety of flood gate vibrations due to wave impacts. *Coastal Engineering*, **170**, 104007. ISSN 03783839. doi:10.1016/j.coastaleng.2021.104007.
- Tieleman, O.C., Tsouvalas, A. and Hofland, B. (2019a). Effect of Compressibility and Surface Waves on the Hydrodynamic Pressures for a Vertical Flood Gate. *Proceedings of the Twenty-ninth (2019) International Ocean and Polar Engineering Conference*, 3349–3356.
- Tieleman, O.C., Tsouvalas, A., Hofland, B., Peng, Y. and Jonkman, S. (2019b). A three dimensional semi-analytical model for the prediction of gate vibrations immersed in fluid. *Marine Structures*, **65**, 134–153. ISSN 09518339. doi:10.1016/j.marstruc.2018.12.007.
- Tieleman, O.C., Vorderegger, R., Hofland, B., Tsouvalas, A. and Jonkman, S.N. (2022). A hybrid semi-analytical and finite element model to predict flood gate vibrations. *To be published*.
- Tsouvalas, A. and Metrikine, A. (2014). A three-dimensional vibroacoustic model for the prediction of underwater noise from offshore pile driving. *Journal of Sound and Vibration*, **333**(8), 2283–2311. ISSN 0022460X. doi:10.1016/j.jsv.2013.11.045.
- Tsouvalas, A. and Metrikine, A. (2016). Noise reduction by the application of an air-bubble curtain in offshore pile driving. *Journal of Sound and Vibration*, **371**, 150–170. ISSN 0022460X. doi:10.1016/j.jsv.2016.02.025.
- Tsouvalas, A., van Dalen, K.N. and Metrikine, A.V. (2015). The significance of the evanescent spectrum in structure-waveguide interaction problems. *The Journal of the Acoustical Society of America*, **138**(4), 2574–2588. ISSN 0001-4966. doi:10.1121/1.4932016.
- Van der Wal, R.J. and De Boer, G. (2004). Downtime Analysis Techniques for Complex Offshore and Dredging Operations. In: *23rd International Conference on Offshore Mechanics and Arctic Engineering, Volume 2*, 93–101. ASMEDC. ISBN 0-7918-3744-0. doi:10.1115/OMAE2004-51113.
- Vorderegger, R. (2019). *Optimization of gate design in the Afsluitdijk based on dynamic wave impact*. Master’s thesis, Faculty of Civil Engineering and Geosciences, Delft University of Technology. doi:http://resolver.tudelft.nl/uuid:41c7361a-e8a0-468e-9113-7afa192126ec.

Wood, D. and Peregrine, D. (1997). Wave impact beneath a horizontal surface. In: *25th International Conference on Coastal Engineering*, 2573–2583.

Zheng, X., Gao, S. and Huang, Y. (2020). Cross-mode couplings for the fatigue damage evaluation of trimodal Gaussian processes. *Ocean Engineering*, **202**(January), 107177. ISSN 00298018.
doi:10.1016/j.oceaneng.2020.107177.